2.2.1. Burned area calculation input variables

Mean fire area can be calculated as equation 3 as fires tend to take on an elliptical reform and spread at varying speeds both with and against the direction of the wind (Albini, 1976; Forestry Canada Fire Danger Group, 1992).

$$\underline{af} = \frac{\frac{\pi}{4 \times L_B} \times (D_T)^2}{10000} \tag{3}$$

Dt is the length of major axis (m), in SEIB-DGVM we use the resolution of establishment site for woody PFTs (Dived) variable. L_B is the length-to-breadth ratio of the elliptical form of fires (Forestry Canada Fire Danger Group, 1992) and calculated PFTs specific, for woody and grass PFTs. L_B can be estimated as a weighted average of $L_{B,tree}$ and $L_{B,grass}$.

$$L_{B,tree} = 1.0 + 8.729 \times \left(1 - e^{-0.03 \times U_{forward}}\right)^{2.155} \tag{4}$$

$$L_{B,grass} = 1.1 + \left(U_{forward}\right)^{0.464} \tag{5}$$

Ignition event $E(n_{ig})$ is the sum of independent calculations of lightning-caused (n_{il}) and human-caused (n_{ih}) fire ignition events, ignoring stochastic variations (Thonicke *et al.*, 2010).

$$E\left(n_{ig}\right) = n_{ih} + n_{il} \tag{6}$$

2.2.2. Ignition events

The LIS/OTD High-Resolution Full Climatology (HRFC) V2.3.2015 (Cecil and Daniel, 2001) data provided frequency of lightning-caused ignition events (n_{il}), actual unit is count/km^2/year then converted into count/ha/year, and gives the annual frequency of total lightning flash rates. Human-caused ignition events (n_{ih}) used population density data obtained from Gridded Population of the World (GPWv4) (CIESIN, 2018), as the default unit is person km^{-2}, we converted it into person/ha.

The population density and lightning flash data detailed information are shown in Table S1 in the Supplement.As the first improvement step, we modified the data format, the GPWv4 (netCDF) and LIS/OTD HRFC (hdf5) data are gridded into 1° grid mesh (360×180) as the SEIB-DGVM requirements for land property (land_prop.txt) input, then converted into text format (.txt), and make sure that the sequence is N90W180, N90W179, ..., N89W180, ..., S90E180, each line corresponds to one grid mesh, so the data structure will be 1 column and 64800 rows, text format files.

The SEIB-DGVM fire module improvement workflow was shown in Figure 3 in the main article, and the orange color inside the dashed box indicates the new input and there is absolute certainty to add another new input that might be considered in the further improvement of SEIB-DGVM. Interestingly, we found a novel discovery in this model improvement process that there will be a huge possibility improvement of SEIB-DGVM in the near future for many research areas because SEIB-DGVM is able to accept any new input as long as it meets the input data requirements and able to process well and can be integrated with the variables in it, so we believed that SEIB-DGVM has a high potential to be a rapid-growing model for analyzing and simulating global vegetation dynamics from many perspectives, needs, and scientific focus areas.

To ensure that the data can be read and processed well by SEIB-DGVM, we visualize it on a global scale and in Siberia, according to the research area as shown in Figure S1, prepared the data in (netCDF) format in 0.5° spatial resolution to be able to compare with the output results of the data in SEIB-DGVM (as the data output from SEIB-DGVM is in 0.5° spatial resolution).

Figure S2 shows the SEIB-DGVM output of Lightning flash rate and Population density and it's the comparison with the original input GPWv4 and LIS/OTD HRFC data. Based on the comparison results we get the high value of coefficients determination (R^2) and correlation coefficients (R) for both data comparison, the value of lightning flash rate comparison is R^2=0.97, R=0.99, and for population density data is R^2=0.93, R=0.97. Although it doesn't produce 100% comparison results, but 97% and 93%, followed by 0.99 and 0.97 correlation coefficients, for

lightning flash rate and population density data comparison shows a strong relationship between the input and output, and these results proved that the SEIB-DGVM was able to read and process the new input well.

Further explanation of the input-output comparison is: the input data has different formats and spatial resolutions, then the first thing we did is data transformation, transformed the data format and regridding the data to 1° grid for SEIB-DGVM input and to 0.5° grid for output comparison, this process we used the Climate Data Operator (CDO) software (Schulzweida, 2019) remapcon operators, first-order conservative remapping that remaps all fields conservatively to a Gaussian N32 grid. We know that the process of remapping or regridding data will produce a bias, moreover multiple-time regridding the same data, and the size of the bias depends on the technique and method used. The method we used in this study is the best method for regridding compared to other methods, as the first- and second-order conservative methods provide an accurate and conservative machine accuracy, completely general, weights can be computed for any type of grid on a sphere, enabling component model developers to use any grid that is suitable for a specific component without being restricted by compatibility with other component model grids in a connected model environment (Jones, 1999).

After the new input is confirmed able to be read and processed properly by SEIB-DGVM, we implement the complete ignition events equation from SPITFIRE (Thonicke *et al.*, 2010) with some model configuration adjustments and environmental factor parameters.

$$N_{il} = I_p \times Lightning\ Flash\ Rate \tag{7}$$

Latham and Williams, (2001) stated that 0.20 of these are cloud-to-ground flashes (CG), and under ideal conditions for igniting fires, their effectiveness is 0.04 (Latham and Schlieter, 1989; Latham and Williams, 2001). *Ip* is an ignition parameter (0.0 – 1.0), and in this study, we used 1.0 because lightning strikes are the primary source of wildfire ignition in Siberia (Sofronov *et al.*, 1998; Ivanova and Ivanov, 2005; Kharuk *et al.*, 2016), with continued regional warming, the role of lightning as a source of wildfire ignition is likely to increase both because of the increased availability of dry fuel as well as from a direct increase in lightning frequency (Kharuk *et al.*, 2022). Research in areas with similar environmental conditions about lightning strikes in the continental USA projects that an increase in air temperature by 1°C leads to an increase in lightning frequency of ~12% (Romps *et al.*, 2014), and for Alaska and northern Canada, lightning ignition was estimated to increase by 90–230% by the end of this century (Hessilt *et al.*, 2021).

Regarding the lightning input dataset on the module, we used one-year and annual data of LIS/OTD HRFC as interannual variability in lightning is generally small (Thonicke *et al.*, 2010).

$$N_{ih} = P_D \times k(P_D) \times \frac{a(N_D)}{100} \tag{8}$$

$$k(P_D) = 30.0 \times e^{-0.5 \times \sqrt{P_D}} \tag{9}$$

After climatic sensitivity ignition, human activity grew to become a stronger factor in controlling fire regimes also due to the construction of the Trans-Siberian Railway and the subsequent development of settlements in remote areas (Ivanova and Ivanov, 2005). Thus, in this improvement, we considered the population density ignition factor also. P_D is the population density (persons km^{-2}), and $a(N_D)$ (ignitions individual^{-1}) is a parameter expressing a person's probability of causing an ignition event (Thonicke *et al.*, 2010). The function forms is supported by Archibald *et al.*, (2009) analysis, that the number of fires in southern Africa tends to rise as population density rises up to roughly 10 kilometers and declines thereafter. At the global scale analysis, Knorr *et al.*, (2014) also discovered that fire frequency rises by 10 to 20% in areas with less than 0.1 persons per km^2 compared to its value in areas with no population. In the SEIB-DGVM, $a(N_D)$ is and user-definable parameter, with a scale of 0.0 – 1.0, and in this study we adjust the value to 0.7 or 70% (total of human and unknown caused fire), as the recent research in eastern Siberia Xu *et al.*, (2022), shown that fires over Yakutia, 31.4 ± 6.8% caused by lightning ignitions, 51.0 ± 6.9% caused by anthropogenic ignitions, and the last 14.4% unknown cause.

2.2.3. Fuel moisture content

Default SEIB-DGVM already has a fuel moisture content equation, and according to Thonicke *et al.*, (2001) we made variable name adjustments as GlobFIRM to make tracking and improvement easier. The fuel moisture content calculation *(m)*, is as follows:

$$m = \frac{frac\ moisture\ litter \times pool\ w1\ runningrecord(1)}{Depth * Wfi} \tag{10}$$

$$m = 0.4994 \times \tilde{m} + 1.02 \tag{11}$$

Fuel moisture content calculation inside SEIB-DGVM (Equation 12) is based on the fuel moisture content calculation in the LPJ-DGVM (Equation 13), where$frac\ moisture\ litter$ is a local parameter of the fraction of litter moisture to soil moisture at the top layer and the default value is 0.5, $pool\ w1\ runningrecord(1)$ is annual soil water content of first soil layer, *Depth* is soil depth (there are 3 soil layers and the depth of each layer is 500 mm, 1000 mm, and 1500 mm, respectively) and *Wfi* is field capacity (Sato *et al.*, 2007). Equation 13 obtained from equation 8 by Viegas *et al.*, (1992), that used to predict the fuel load on the Moisture module inside the BEHAVE system.

In the fire module improvement, we added the equation of relative moisture content *(ω_o)* of the fuel load:

$$\omega_o = e^{(-(\alpha_{av} \times fuel\ load) \times NI)} \tag{12}$$

The values of α_{av} ($^oC^{-2}$) are average of inverse proportion to their surface-area-to-volume ratios of each fuel classes, with $\alpha_{1h} = 1.0 \times 10^{-3}$, $\alpha_{10h} = 5.42 \times 10^{-5}$, and $\alpha_{100h} = 1.49 \times 10^{-5}$. We used the average value of $(\alpha_{1h}, \alpha_{10h}, and\ \alpha_{100h})$ because SEIB-DGVM classifies fuel load by biomass type: litter trunk, litter leaf, and aboveground biomass, and for LPJ-DGVM SPTIFIRE allocated among four fuel classes: 1-h (leaves and twigs, i.e. leaf mass plus 4.5% of the carbon stored as heartwood (HW) and the sapwood (SW), respectively), 10-h (small branches, i.e. 7.5% of HW and SW), 100-h (large branches, i.e. 21% of HW and SW) and 1000-h (boles or trunks, i.e. 67% of HW and SW) (Thonicke *et al.*, 2010). The consumption of 1000-h fuels is not considered in the calculation of moisture content because does not influence fire spread or intensity (Pyne *et al.*, 1996).

NI is an abbreviation of Nesterov Index ($^\circ C^2$), is a cumulative function of daily maximum temperature T_{max} and dew-point temperature T_{dew} ($^\circ C$):

$$NI = \sum \quad T_{max} \times (T_{max} - T_{dew}) \tag{13}$$

$$NI = \sum \quad T_{max} \times \left(T_{max} - (T_{min} - 4.0)\right) \tag{14}$$

We approximate T_{dew} by (T_{min}−4), where T_{min} is the daily minimum temperature (Running *et al.*, 1987), same approach used by (Venevsky *et al.*, 2002), and (Thonicke *et al.*, 2010).

2.2.4. Fire Danger Index

Fire Danger Index *(FDI)* is the probability that an ignition event will start a fire and can be calculated by combining the relative moisture content equation *(ω_o)* (Equation 14), the fire spread probability equation *(P_{spread})* (Equation 17), and also depends on fire weather conditions as described by NI (Equation 16). Moisture extinction (m_e) is PFT-specific disturbance parameter that indicates the proportion of litter moisture extinction due to fire.

$$P_{spread} = \left\{1 - \frac{\omega_o}{m_e}, \omega_o \leq m_e\ 0, \omega_o > m_e \right\} \tag{15}$$

$$FDI = max\left(0, \left(1 - \frac{1}{m_e} \times e^{-((\alpha_{av} \times fuel\ load) \times NI)}\right)\right) \quad (16)$$

Equation 18 will produce the Fire Danger Index *(FDI)* value if there is enough fuel load that satisfies the minimum threshold (200 g C m^{-2}), and FDI will be zero if there is no fuel or the fuel has a high moisture content that is unable to be ignited.

2.2.5. Rate of spread

The rate of Spread (ROS) is the predicted speed of the fire in the front or head of the fire, where it spreads the fastest, is known as which accounts for both crowning and spotting and can be obtained using Rothermels equations (Rothermell, 1972; Wilson, 1982; Pyne *et al.*, 1996). We also implemented the complete rate of spread equations as SPITFIRE (Thonicke *et al.*, 2010) as we were able to add all of the needed parameters, integrate it, and create new variables on SEIB-DGVM.

The forward and backward fire rate of spread $ROS_{f,surface}$ and $ROS_{b,surface}$ (m min^{-1}) respectively, can be obtained by:

$$ROS_{f,surface} = \frac{I_R \times \xi \times (1 + \phi_w)}{p_b \times \varepsilon \times Q_{ig}} \quad (17)$$

$$ROS_{b,surface} = ROS_{f,surface} \times e^{-0.012 \times U_{forward}} \quad (18)$$

I_R is the reaction intensity, the energy that is released per unit fire front area (kJm^{-2} min^{-1}); ξ is the propagating flux ratio, the percentage of I_R that causes nearby fuel particles to heat up and ignite; ϕw is a multiplier that takes into consideration how wind affects the effective value of ξ; ρb is the fuel bulk density (kgm^{-3}), assigned by PFT-specific parameter (Table 1); ε is the effective heating number, the percentage of a fuel particle that reaches ignition temperature at the beginning of flame combustion; and Q_{ig} is the heat of pre-ignition, the heat needed to ignite a specific mass of fuel (kJ kg^{-1}). The ROS variable calculation details are explained in more detail in Appendix A.

The estimated fire duration can also be calculated based on the fire danger index, using the following equation:

$$t_{fire} = \frac{241}{1 + 240 \times e^{-11.06 \times FDI}} \quad (19)$$

2.2.6. Fire fraction and intensity

The surface fire intensity, $I_{surface}$ (kW m^{-1}) is the product of the forward rate of fire spread $ROS_{f,surface}$, fuel consumption *FC*, fuel heat content *h,* and area burnt fraction $A_{b,frac}$ (Byram, 1959).

$$I_{surface} = h \times \frac{\sum FC}{1000 \times A_{b,frac}} \times \frac{ROS_{f,surface}}{60} \quad (20)$$

$$A_{b,fraction} = \frac{A_b}{A} \quad (21)$$

FC is fuel consumption in a surface fire (gDM m^{-2}), and calculated using empirical equations as fuel moisture function of the fuel load (Peterson and Ryan, 1986), this equation has been adjusted for SEIB-DGVM as there is no fuel classification based on the length of combustion.

2.2.7. Fire damage to plants

The SPITFIRE module is very detailed in its classification of fire spread, ranging from surface fires to crown scorch caused by surface fire. The scorch height *SH* of the fire can be obtained by the following equation (Peterson and Ryan, 1986; Agee, 1997; Dickinson and Johnson, 2001):

$$SH = F \times \left(I_{surface}\right)^{0.667} \tag{22}$$

F is PFT-specific parameter of the crown scorch equation (Table 1). Assuming a cylindrical crown, the crown scorch fraction (CK) impacted by a fire can be obtained using the following formula:

$$CK = \frac{SH - T_H + CL}{CL} \tag{23}$$

T_H is the individual tree height of woody PFT, *CL* is crown length, and the value is provided by PFT-specific parameters (Table 1). Post-fire tree mortality is caused by the cambium damage, and crown damage is caused by bark heating. Those causes are assumed to act independently, so the total probability of mortality P_m *is* determined by the probability of crown damage mortality $P_m(CK)$ and cambial damage $P_m(\tau)$.

$$P_m = P_m(\tau) + P_m(CK) - \left(P_m(\tau) \times P_m(CK)\right) \tag{24}$$

The probability of crown damage mortality $P_m(CK)$ is obtained by:

$$P_m(CK) = r(CK) \times CK^p \tag{25}$$

r(CK) is the crown damage resistance factor, and *p* is Woody PFTs parameter, the values of each parameter are described in Table 1 (Peterson and Ryan, 1986; Williams *et al.*, 1998; Cochrane, 2003).

Probability of cambial damage mortality $P_m(\tau)$:

$$P_m(\tau) = \left\{0, \frac{\tau_l}{\tau_c} \leq 0.22\ 0.563 \times \frac{\tau_l}{\tau_c} - 0.125, \frac{\tau_l}{\tau_c} > 0.22\ 1, \frac{\tau_l}{\tau_c} \geq 2.0\right\} \tag{26}$$

τ_l is the residence time of the fire, τ_c is the critical time of cambial damage, so τ_l/τ_c is the ratio of fire residence time to the cambial damage (Peterson and Ryan, 1986). The value of τ_l is dependent on I_R, as provided by the fire spread model (Rothermell, 1972; Wilson, 1982), described in Appendix A. The critical time of cambial damage τ_c (min), depends on the bark thickness (cm) (Peterson and Ryan, 1986).

$$\tau_c = 2.9 \times BT^2 \tag{27}$$

$$BT = par_1 \times DBH + par_2 \tag{28}$$

BT calculated from the diameter at breast height, *DBH* (cm), and par_1 and par_2 are PFT-specific parameters (Table 1). Generally, during a fire, all leaf biomass of grass, all leaf biomass of dead and surviving trees, half of the trunk biomass of dead trees, and half of the litter pool are burned (classified into surface fire and crown scorch), while the remaining biomass of dead trees is transformed into litter. In response to fire, the phenology phase of all grass PFTs changes to dormant (they reenter the growth phase as described previously in the section titled 'Phenology'). If the stock resource of grass PFTs (*gmassstock*) does not satisfy the minimum value (50 g DM m–2) after fire, the deficit is supplemented by litter (Sato *et al.*, 2007). The fraction of individual trees killed in a fire also depends on PFT fire resistance (M3, Table 1).

2.2.8. Trace gas and aerosol emissions

Trace gas and aerosol emissions estimation is referred to the Fire Modeling Intercomparison Project (FireMIP) protocols (Li *et al.*, 2019), the comprehensive study comparison of nine dynamic global vegetation models (DGVMs) and produced important estimation for long-term and large-scale fire emissions. By using FireMIP protocol reference, SEIB-DGVM SPITFIRE improved to output PFT-level fire emissions.

Trace gas and aerosol emissions are the result of the total amount of burned biomass, the sum of dead and live fuel consumption as the result of surface fire and crown scorch. Trace gas emissions are estimated based on fire

carbon emissions, vegetation characteristics from DGVMs, and fire emissions factors. Fire emissions of trace gas and aerosol for each species *i* and PFT *j*, $E_{i,j}$ (g species m^{-2}) are estimated based on Andreae and Merlet, (2001):

$$E_{i,j} = EF_{i,j} \times \frac{CE_j}{C} \tag{29}$$

$EF_{i,j}$ (g species (kg dry matter (DM))$^{-1}$) is PFT specific emission factor, CE_j is the combusted biomass of PFT_j due to the fire (g C m^{-2}), and C is the unit conversion factor from carbon to dry matter, $C = 0.5 \times 10^3 gC(kg\ DM)^{-1}$. The Emission factors *(EF)* used in this study are based on Andreae and Merlet, (2001), and the updated pyrogenic emissions species by various types of biomass burning (Andreae, 2019) (Table S2 in the Supplement).

DGVMs generally simulate vegetation as a combination of PFTs in a given grid location to represent plant function at a global scale, instead of land cover types (Li *et al.*, 2019). In this, we classified the PFTs with the LCTs to integrate the emission factors of each LCTs for trace gas and aerosol emissions estimation process. TrBE and TrBR are classified as Tropical Forest; TeNE, TeBE, and TeBS are classified as Temperate Forest; BoNE, BoNS, and BoBs are classified as Boreal Forest, and the last is Teh and TrH are classified as Grassland/ Savana, SEIB-DGVM didn't classify crop PFTs so cropland LCTs will not be used.

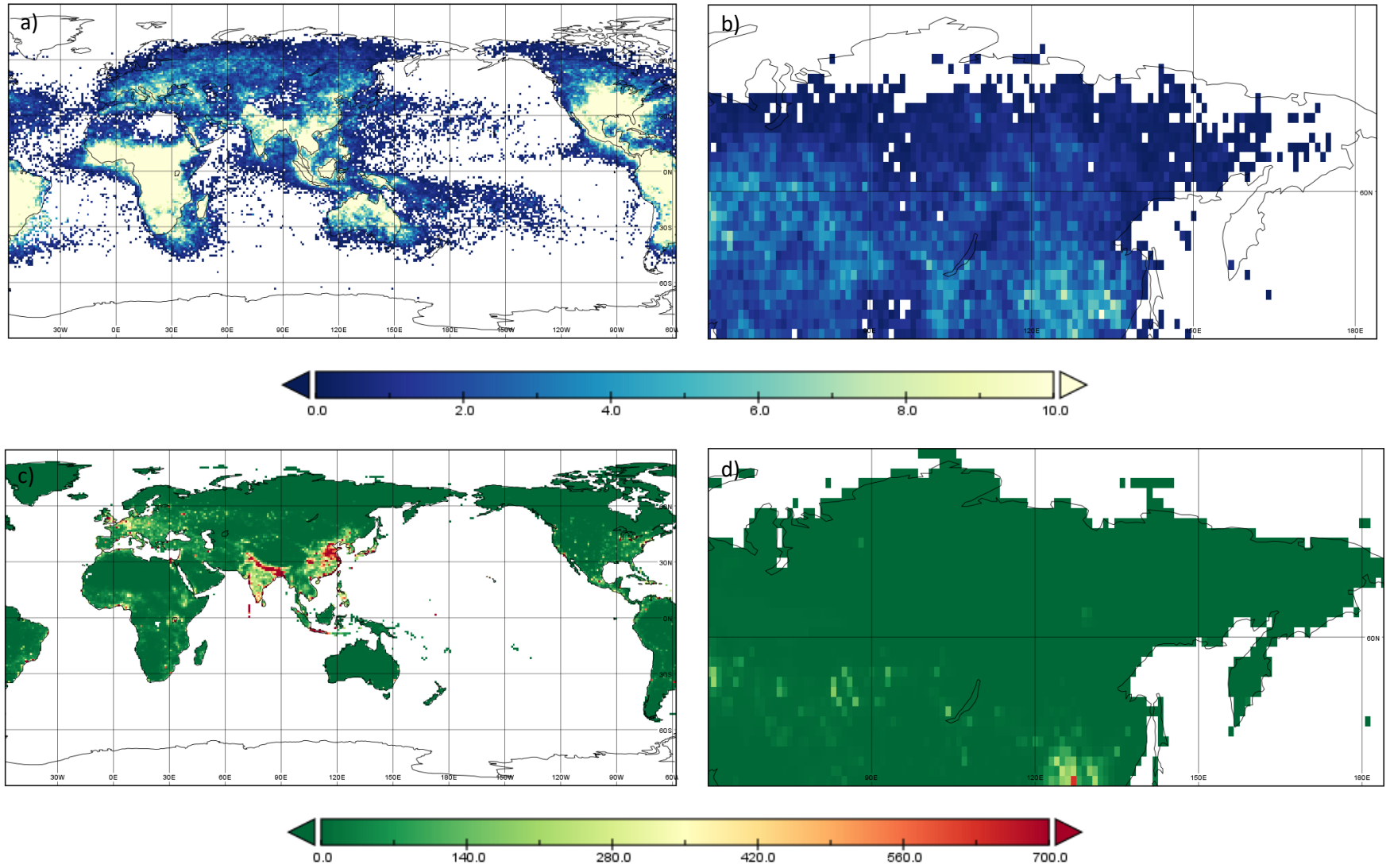

Figure S1. Lightning flash rate and Population density input data: a) LIS/OTD HRFC global view b) LIS/OTD HRFC Siberian view c) GPWv4

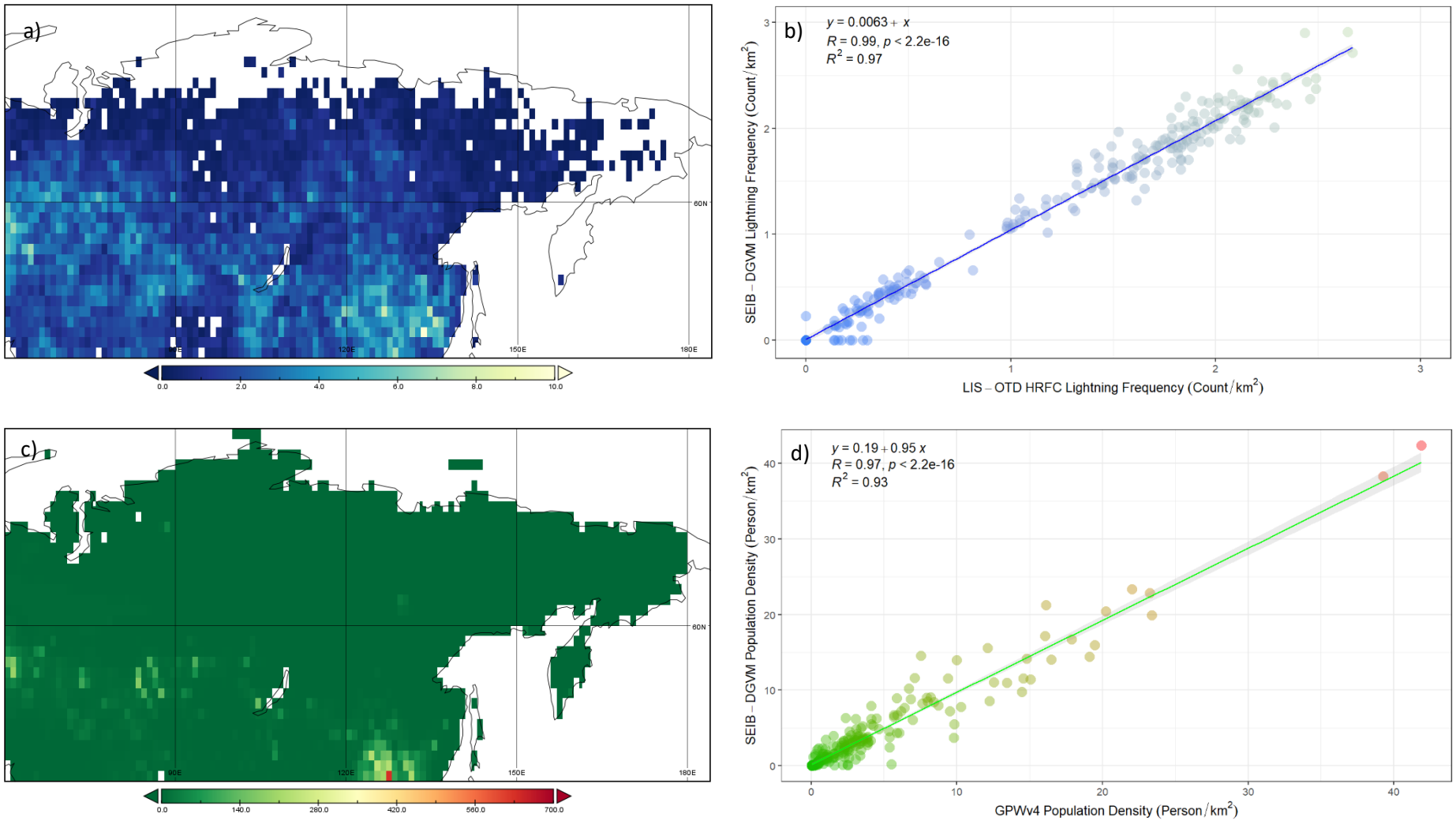

Figure S2. Lightning flash rate and Population density output and comparison results: a) LIS/OTD HRFC output b) LIS/OTD HRFC input-output comparison c) GPWv4 output d) GPWv4 input-output comparison

Table S1. Population and lightning input data information

Variable	Unit	Product	Spatial resolution	Temporal resolution	Temporal coverage	Reference
Population density	person/km^2	Gridded Population of the World (GPWv4)	2.5 arc-minute	Annual	2000-2020	(CIESIN, 2018)
OTD Flash Rate	count/km^2/year	LIS/OTD High Resolution Full Climatology (HRFC) V2.3.2015	0.5 degree	Annual	2015	(Cecil and Daniel, 2001)

Table S2. Emission factors (g species (kg DM^{-1}) for land cover types (LCTs) (Andreae and Merlet, 2001; Andreae, 2019)

No.	Species	PFT parameter abbreviation	Grassland/ savana	Tropical forest	Temperate forest	Boreal forest	Cropland
1	CO_2	ES1	1647	1613	1566	1549	1421
2	CO	ES2	70	108	112	124	78
3	CH_4	ES3	2.5	6.3	5.8	5.1	5.9
4	NHMC	ES4	5.5	7.1	14.6	5.3	5.8
5	H_2	ES5	0.97	3.11	2.09	1.66	2.65
6	NO_x	ES6	2.58	2.55	2.9	1.69	2.67
7	N_2O	ES7	0.18	0.2	0.25	0.25	0.09
8	$PM_{2.5}$	ES8	7.5	8.3	18.1	20.2	8.5
9	TPM	ES9	8.5	10.9	18.1	15.3	11.3
10	TPC	ES10	3.4	6	8.4	10.6	5.5
11	OC	ES11	3.1	4.5	8.9	10.1	5
12	BC	ES12	0.51	0.49	0.66	0.5	0.43
13	SO_2	ES13	0.51	0.78	0.75	0.75	0.81
14	C_2H_6 (ethane)	ES14	0.42	0.94	0.71	0.9	0.76
15	CH_3OH (methanol)	ES15	1.48	3.15	2.13	1.53	2.63
16	C_3H_8 (propane)	ES16	0.14	0.53	0.29	0.28	0.2

No.	Species	PFT parameter abbreviation	Grassland/ savana	Tropical forest	Temperate forest	Boreal forest	Cropland
17	C_2H_2 (acetylene)	ES17	0.34	0.43	0.35	0.27	0.32
18	C_2H_4 (ethylene)	ES18	1.01	1.11	1.22	1.49	1.14
19	C_3H_6 (propylene)	ES19	0.49	0.86	0.67	0.66	0.48
20	C_5H_8 (isoprene)	ES20	0.12	0.22	0.19	0.07	0.18
21	$C_{10}H_{16}$ (terpenes)	ES21	0.1	0.15	1.07	1.53	0.03
22	C_7H_8 (toluene)	ES22	0.2	0.23	0.43	0.32	0.18
23	C_6H_6 (benzene)	ES23	0.34	0.38	0.46	0.52	0.31
24	C_8H_{10} (xylene)	ES24	0.09	0.09	0.17	0.1	0.09
25	CH_2O (formaldehyde)	ES25	1.33	2.4	2.22	1.76	1.8
26	C_2H_4O (acetaldehyde)	ES26	0.86	2.26	1.2	0.78	1.82
27	C_3H_6O (acetone)	ES27	0.47	0.63	0.7	0.61	0.61
28	$C_3H_6O_2$ (hydroxyacetone)	ES28	0.52	1.13	0.85	1.48	1.74
29	C_6H_5OH (phenol)	ES29	0.37	0.23	0.33	2.96	0.5
30	NH_3 (ammonia)	ES30	0.91	1.45	1	2.82	1.04
31	HCN (hydrogen cyanide)	ES31	0.42	0.38	0.62	0.81	0.43
32	MEK/2-butanone	ES32	0.13	0.5	0.23	0.15	0.6
33	CH_3CN (acetonitrile)	ES33	0.17	0.51	0.23	0.3	0.25

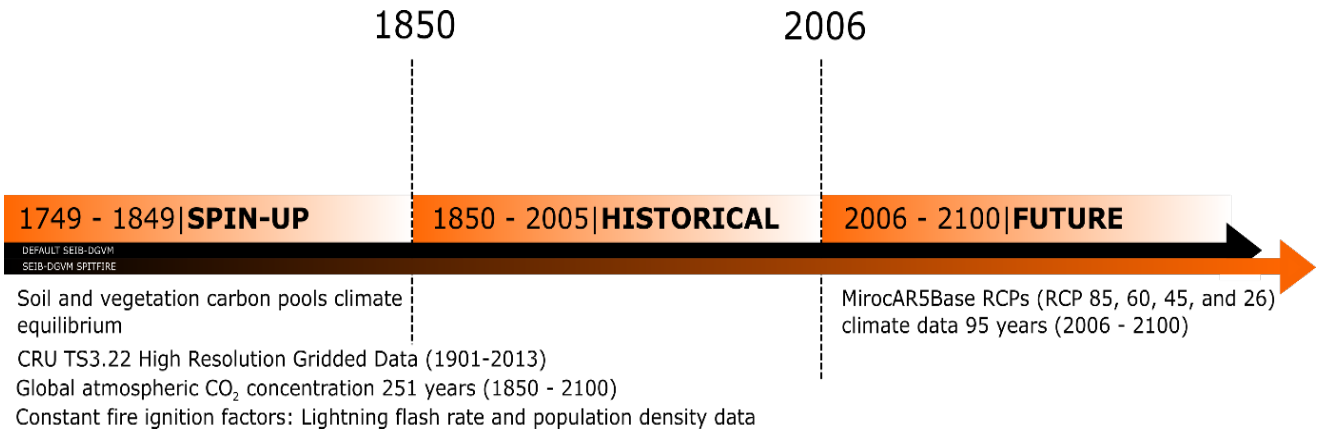

Figure S3. SEIB-DGVM SPITFIRE simulation protocols

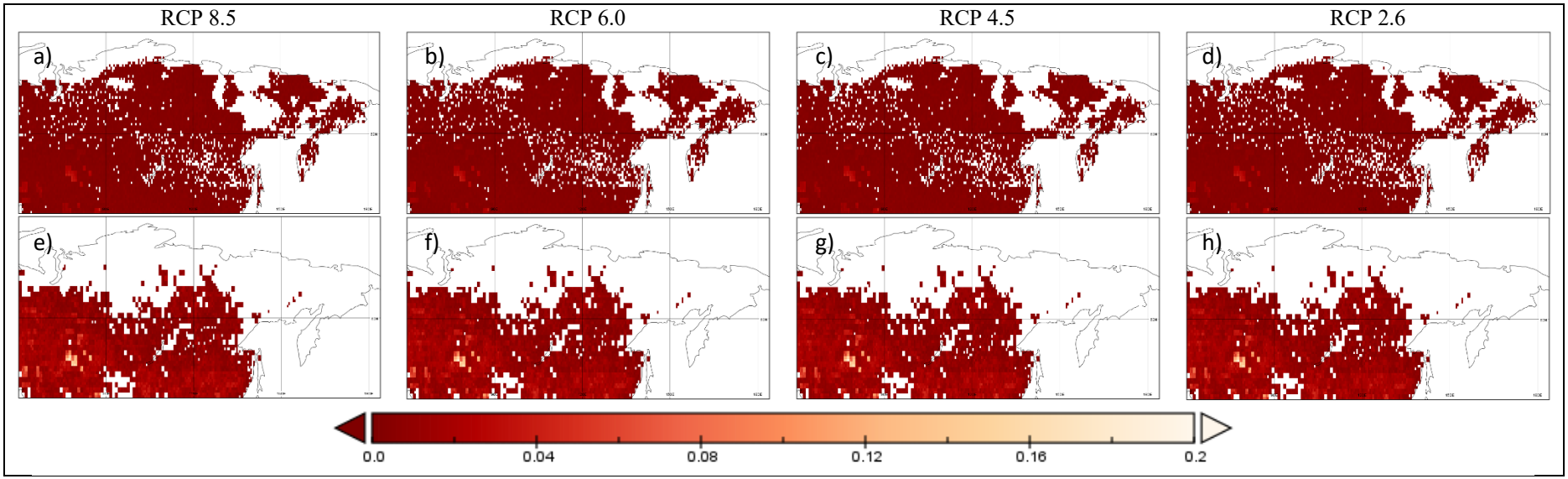

Figure S4. Annual average burned fraction maps (2006-2100) comparison under different RCP scenarios: a-d) SEIB-DGVM Default Fire Module, e-h) SEIB-DGVM SPITFIRE Module

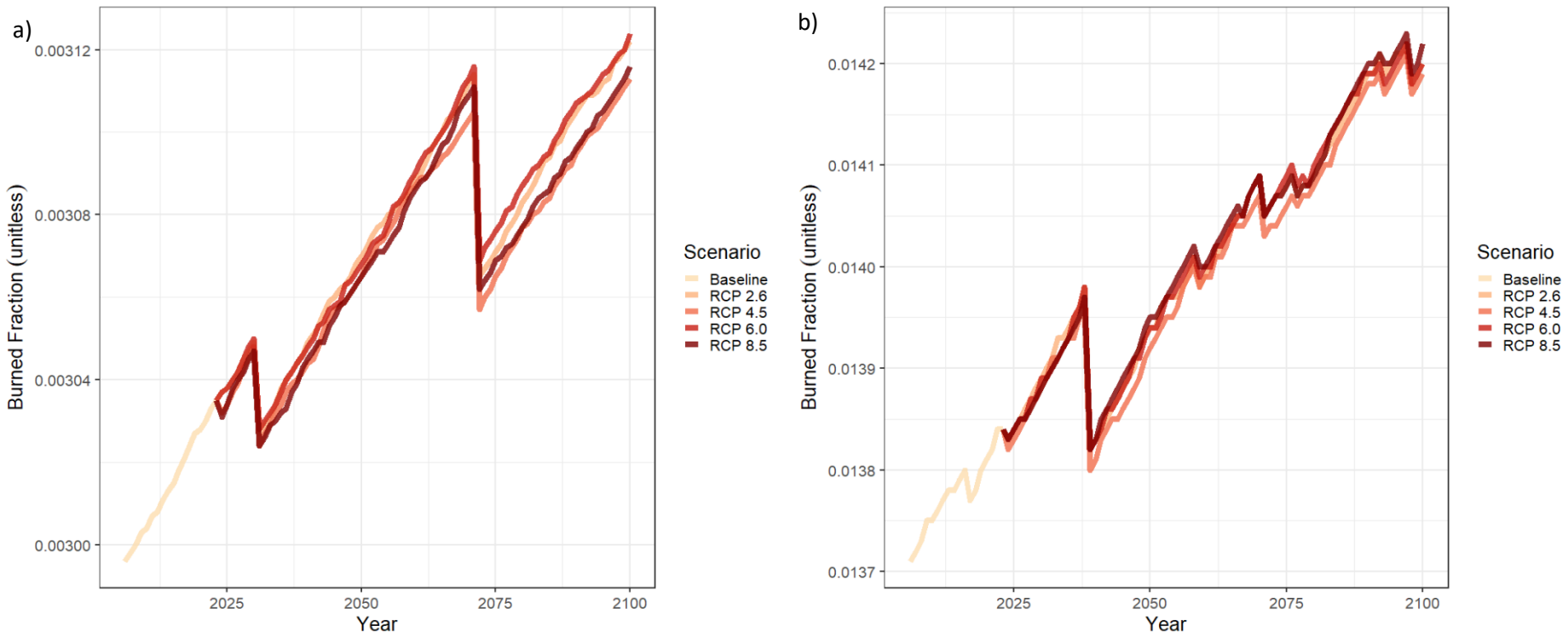

Figure S5. Annual average burned fraction graph (2006-2100) comparison under different RCP scenarios: a) SEIB-DGVM Default Fire Module, b) SEIB-DGVM SPITFIRE Module

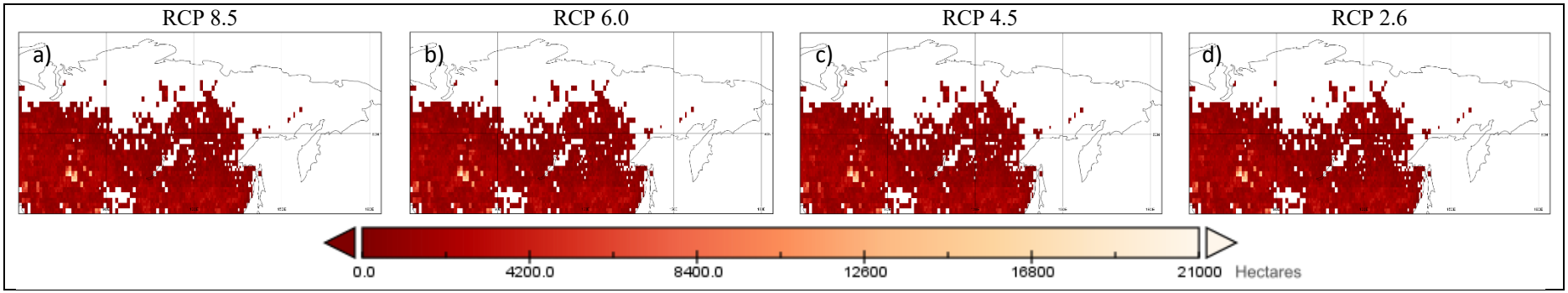

Figure S6. SEIB-DGVM SPITFIRE annual average burned area maps (2006-2100) comparison under different RCP scenarios

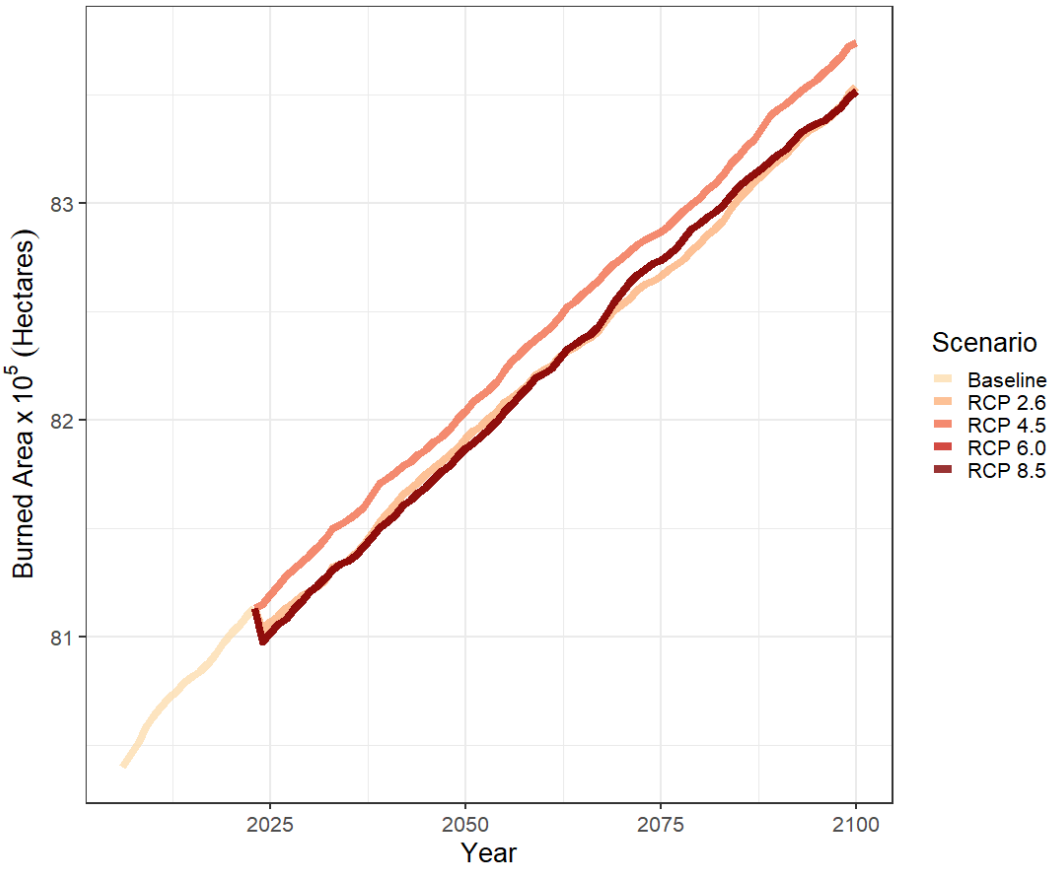

Figure S7. SEIB-DGVM SPITFIRE annual burned area graph (2006-2100) comparison under different RCP scenarios

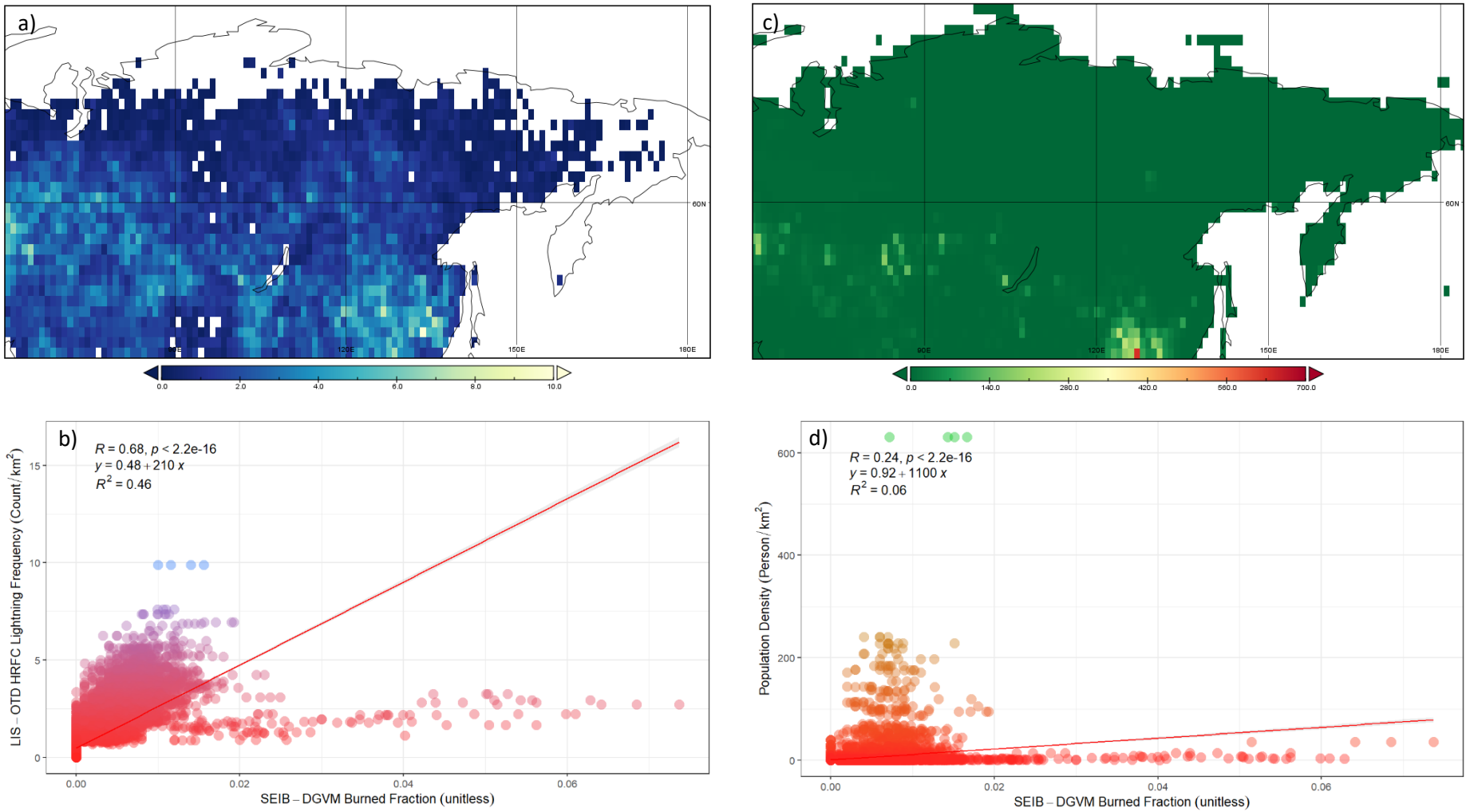

Figure S8. Burned fraction, lightning and population variable comparison: a) Lightning flash rate map, b) Lightning flash rate and burned fraction correlation graph, c) Population density map, b) Population density and burned fraction correlation graph

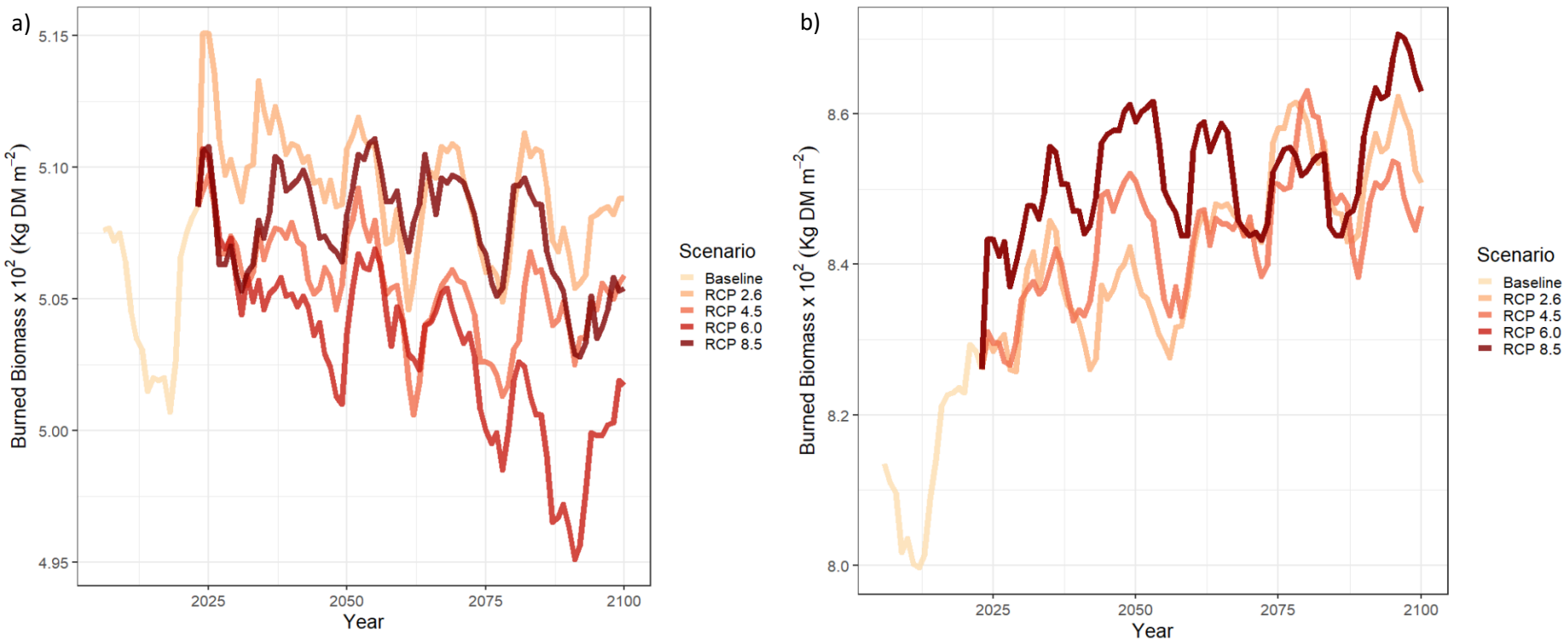

Figure S9. Annual average burned biomass graph (2006-2100) comparison under different RCP scenarios: a) SEIB-DGVM Default Fire Module, b) SEIB-DGVM SPITFIRE Module

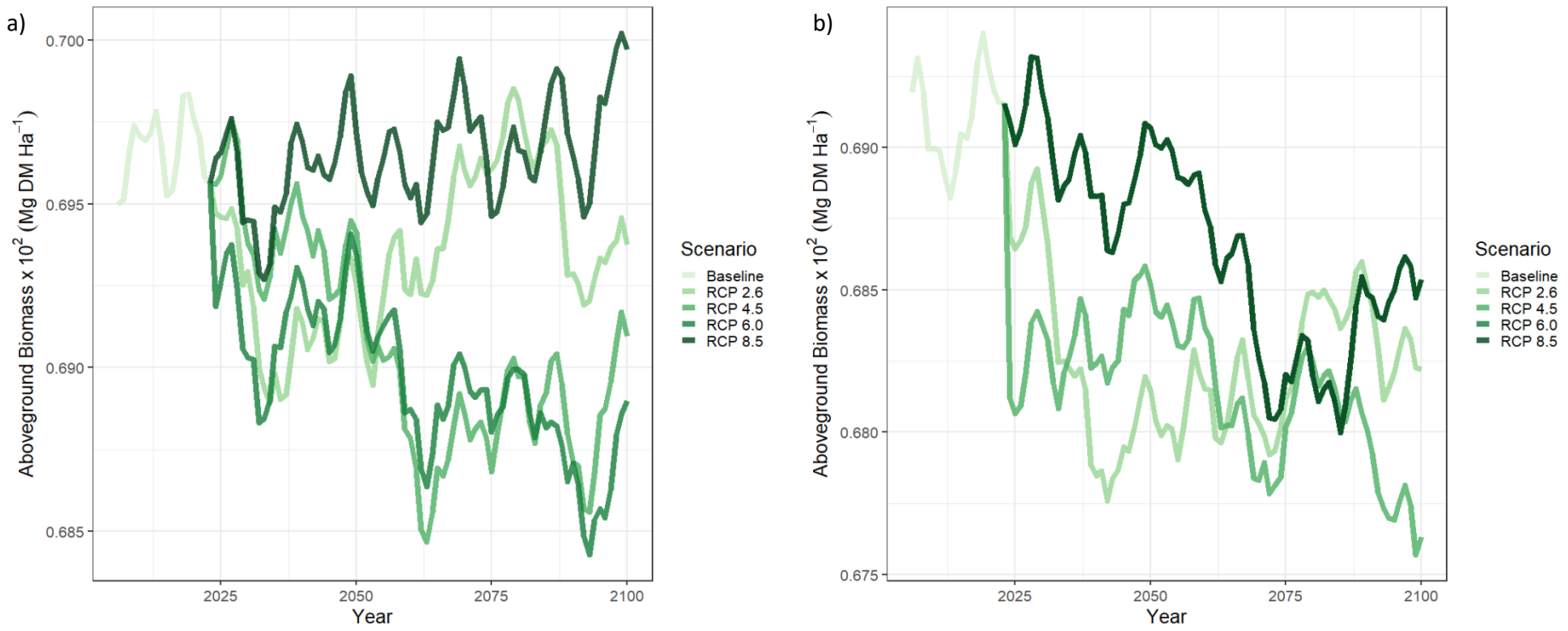

Figure S10. Annual average aboveground biomass graph (2006-2100) comparison under different RCP scenarios: a) SEIB-DGVM Default Fire Module, b) SEIB-DGVM SPITFIRE Module

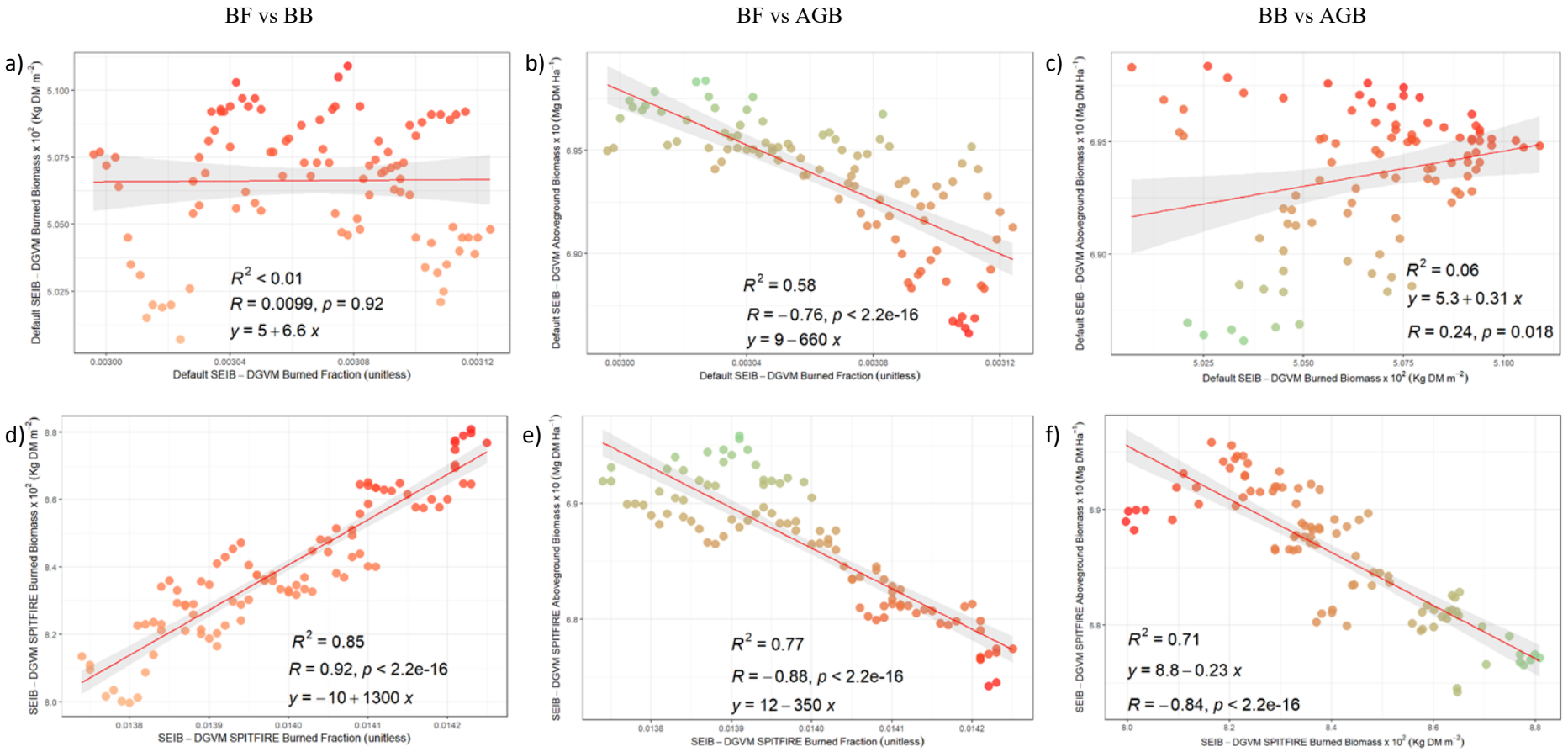

Figure S11. Figure Fire and vegetation product comparison under baseline climate product (CRU TS.3.22): a-c) SEIB-DGVM Default Fire Module, d-f) SEIB-DGVM SPITFIRE Module. BF: burned fraction, BB: burned biomass, and AGB: aboveground biomass

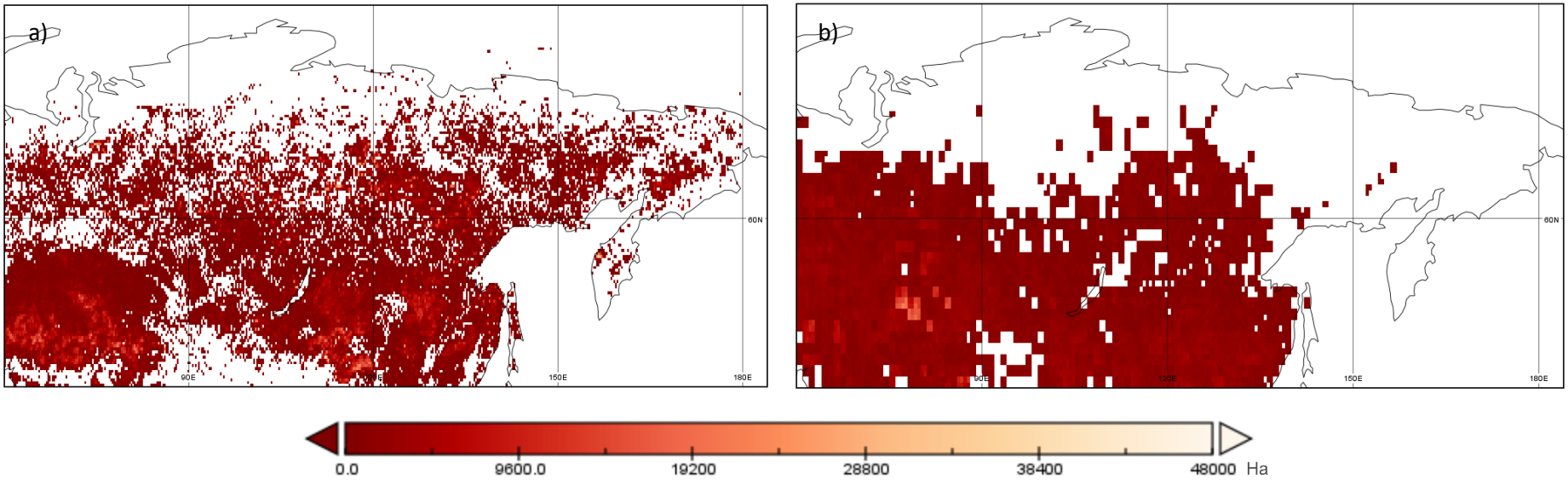

Figure S12. Annual average of burned area (1996-2016) maps: a) GFED4 product, b) SEIB-DGVM SPITFIRE product

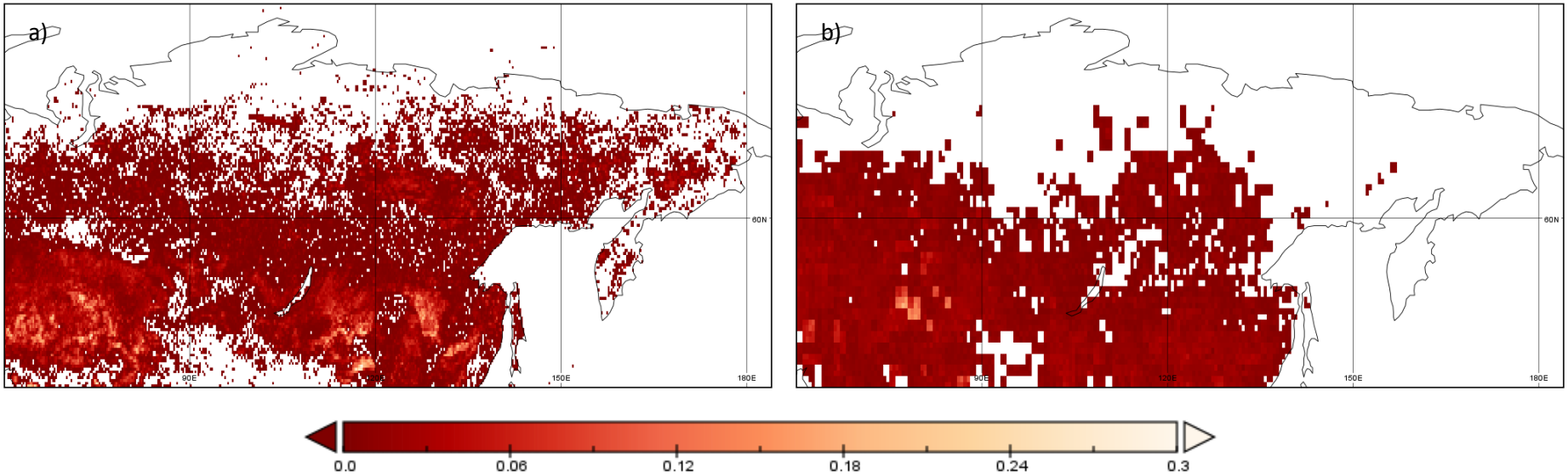

Figure S13. Annual average of burned fraction (1997-2016) maps: a) GFED4s product, b) SEIB-DGVM SPITFIRE product

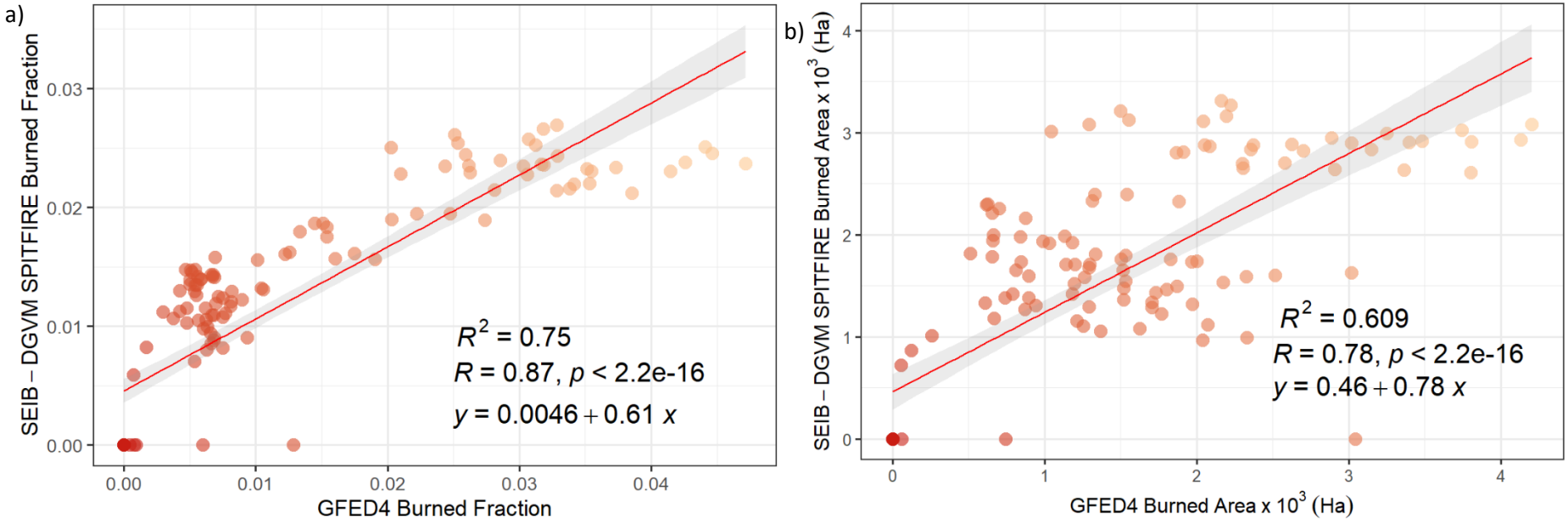

Figure S14. GFED4s burned fraction data and GFED4 burned area data spatial average comparison with SEIB-DGVM SPITFIRE module product under baseline climate product (CRU TS.3.22): a) burned fraction comparison, b) burned area comparison

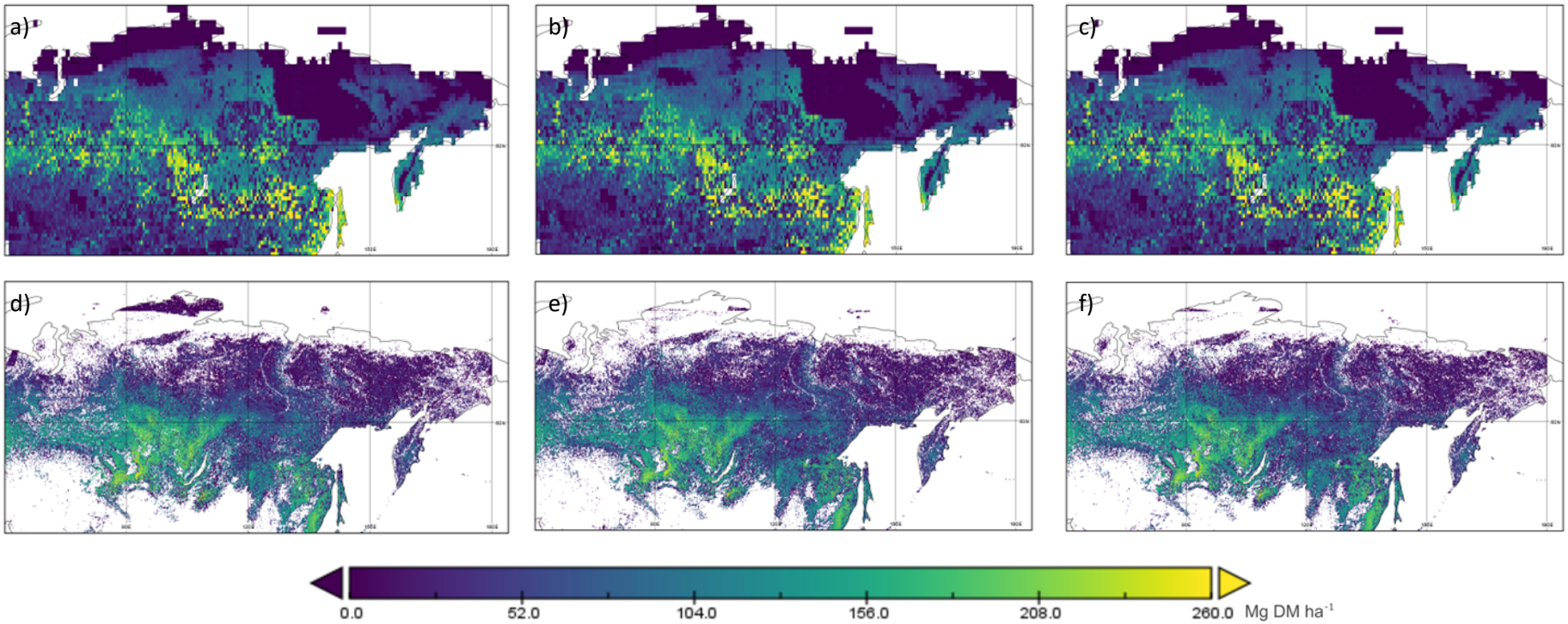

Figure S15. Figure Annual average of aboveground biomass maps (Mg DM Ha^{-1}): a) SEIB-DGVM SPITFIRE 2010, b) SEIB-DGVM SPITFIRE 2017, c) SEIB-DGVM SPITFIRE 2018, d) ESA Biomass Climate Change Initiative 2010, e) ESA Biomass Climate Change Initiative 2017, f) ESA Biomass Climate Change Initiative 2018

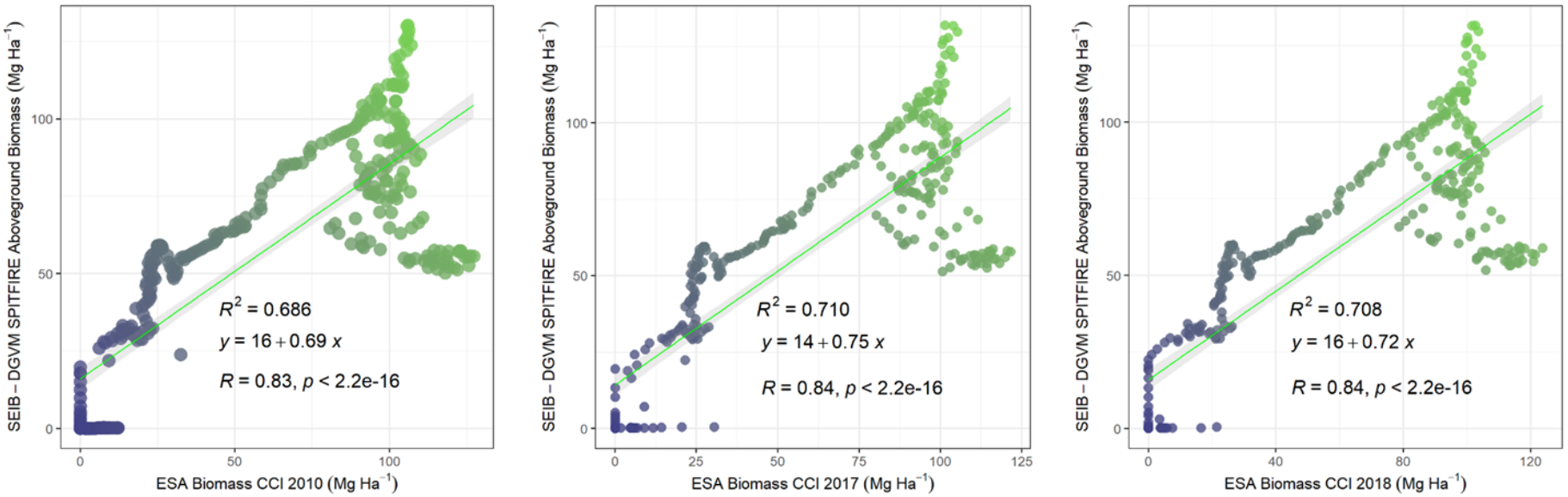

Figure S16. Aboveground biomass spatial average comparison of SEIB-DGVM SPITFIRE module product under baseline climate product (CRU TS.3.22) with ESA Biomass Climate Change Initiative aboveground biomass data (2010, 2017, and 2018)

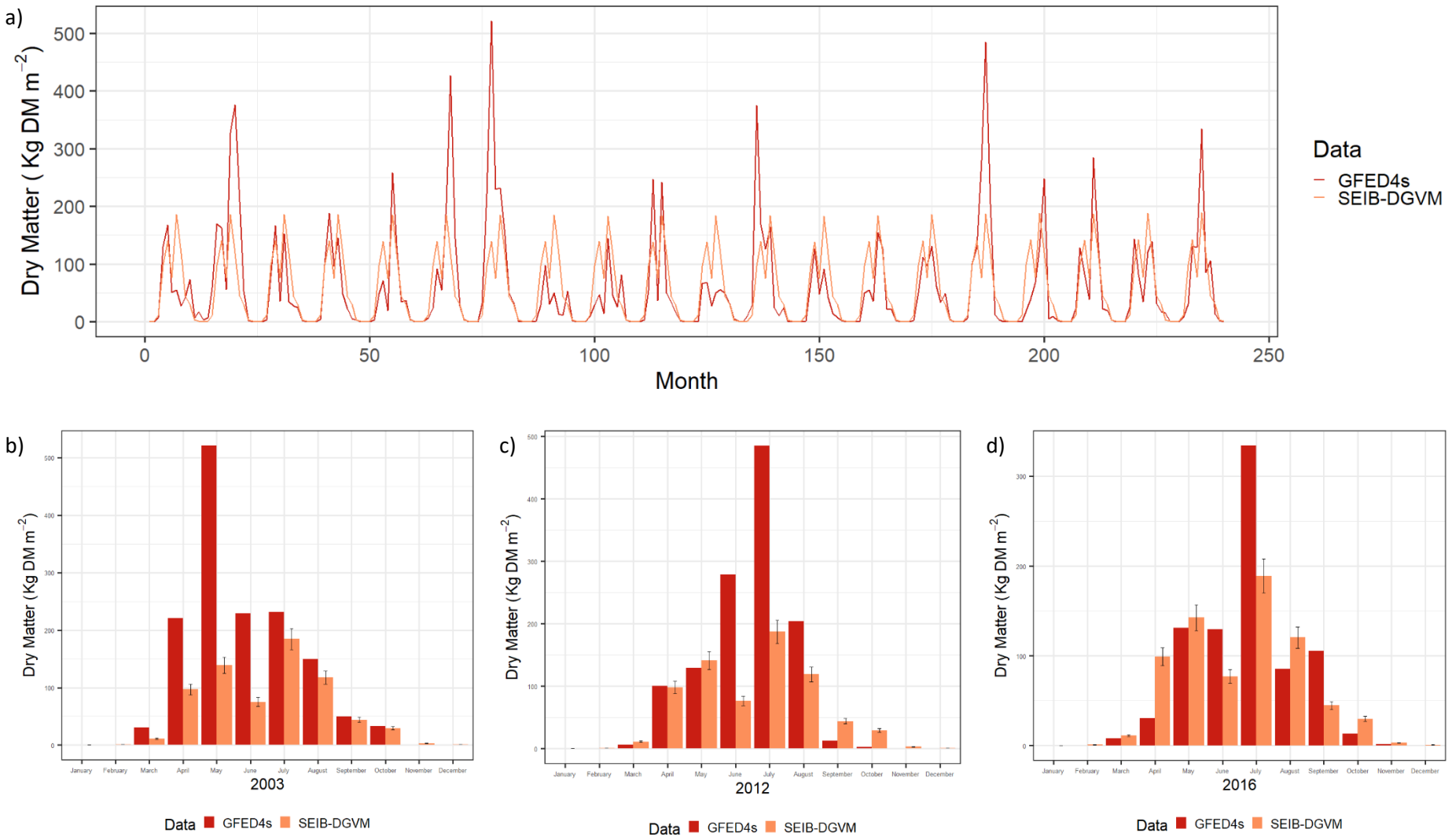

Figure S17. Monthly Dry Matter Emission data comparison of GFED4s and SEIB-DGVM SPITFIRE: a) 1997-2016, b) 2003, c) 2012, d) 2016

Table S3. Annual CO_2 emissions data from GFED4s (Siberia and BOAS), GBEI, and SEIB-DGVM SPITFIRE product (1 x 10^{13} g CO_2)

Year	Siberia			BOAS
	GFED4s	SEIB-DGVM	GBEI	GFED4s
1997	85.9423	75.152	n.a	30
1998	212.3127	75.308	n.a	89
1999	78.2312	75.370	n.a	32
2000	91.2028	76.195	n.a	35
2001	90.7241	76.745	42.49	32
2002	146.7248	76.749	58.29	51
2003	218.6563	76.596	125.1	88
2004	42.2935	76.899	43.7	14
2005	59.1899	77.200	36.37	21
2006	101.7702	77.311	64.84	43
2007	52.6425	76.901	32.62	18
2008	139.1379	76.664	89.25	57
2009	59.2727	75.962	50.47	21
2010	69.6919	76.199	41.26	28
2011	80.1802	75.802	71.73	32
2012	181.7223	75.788	126.8	67
2013	77.3021	75.949	41.23	26
2014	110.0743	76.667	71.46	41
2015	90.7468	77.103	49.86	33
2016	124.9715	77.701	70.33	46
2017	n.a	77.992	46.49	n.a
2018	n.a	77.978	55.51	n.a
2019	n.a	78.076	70.98	n.a
2020	n.a	77.817	60.8	n.a
Average	105.64 ± 50.69	76.41 ± 0.87	62.48 ± 26.09	40.2 ± 21.12

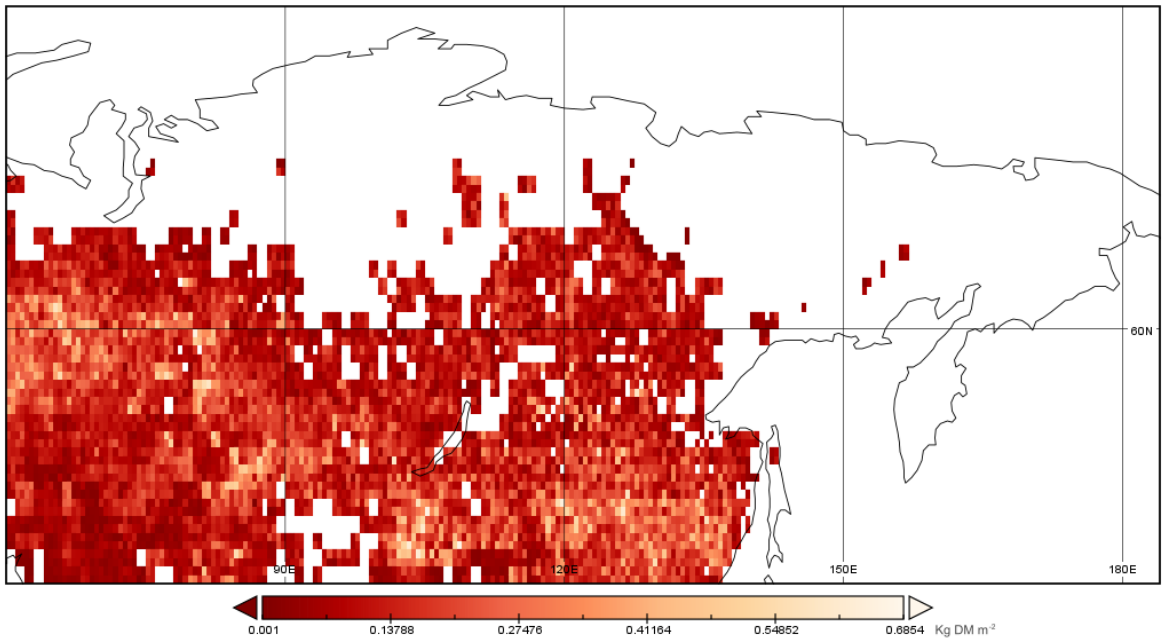

Figure S18. Annual average map of SEIB-DGVM SPITFIRE dry matter emission (1997-2016)

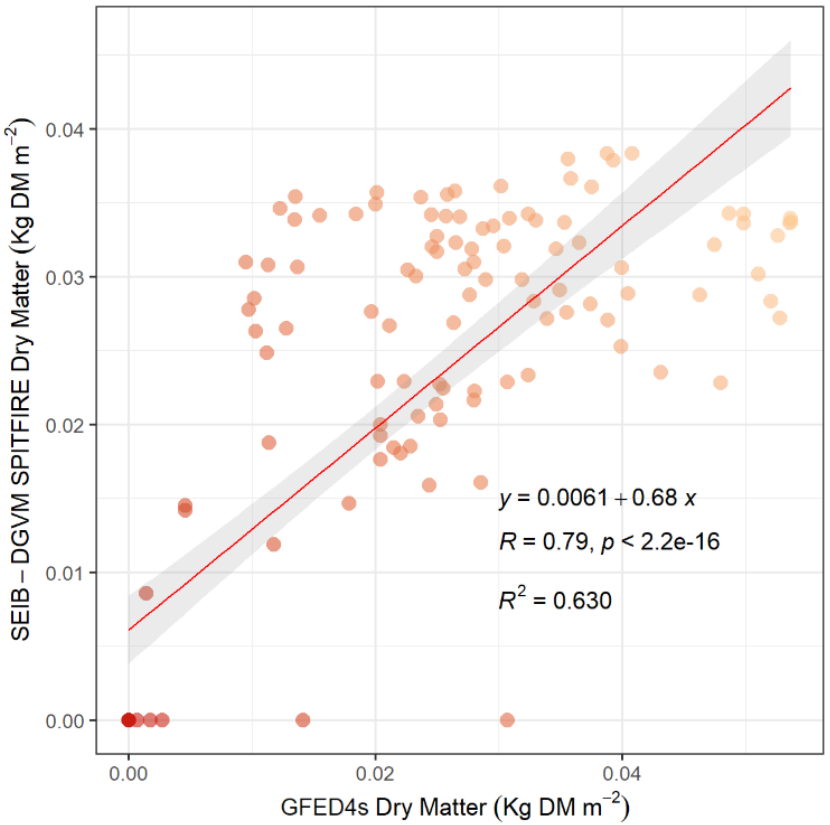

Figure S19. Annual average dry matter emission (1997 - 2016) comparison between GFED4s and SEIB-DGVM SPITFIRE product under baseline climate product (CRU TS.3.22)

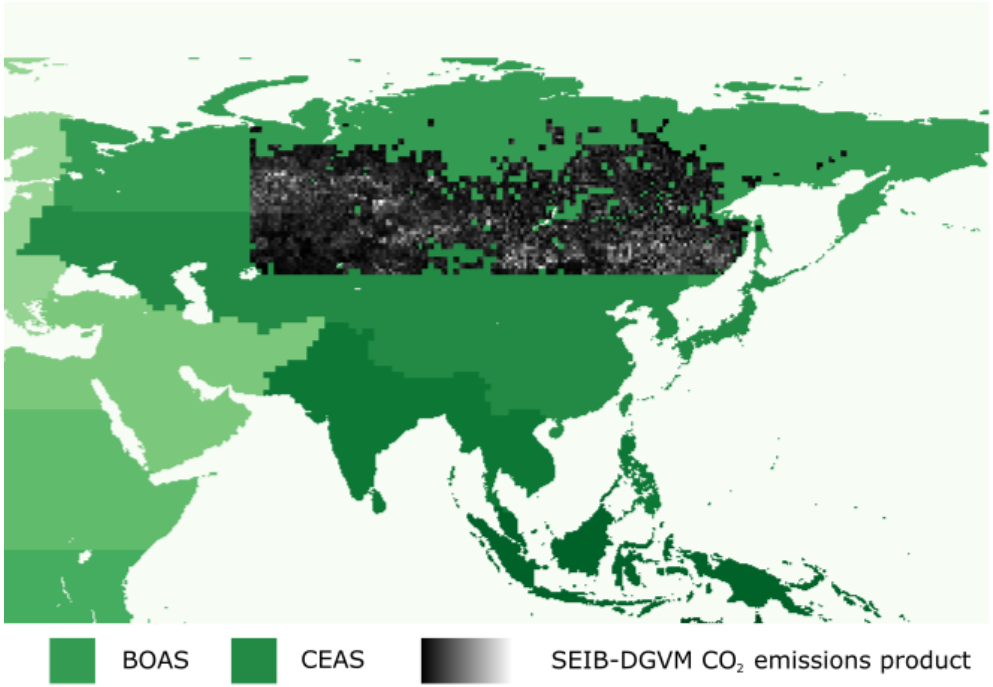

Figure S20. GFED basis region and SEIB-DGVM output area map comparison
BOAS: Boreal Asia. CEAS: Central Asia

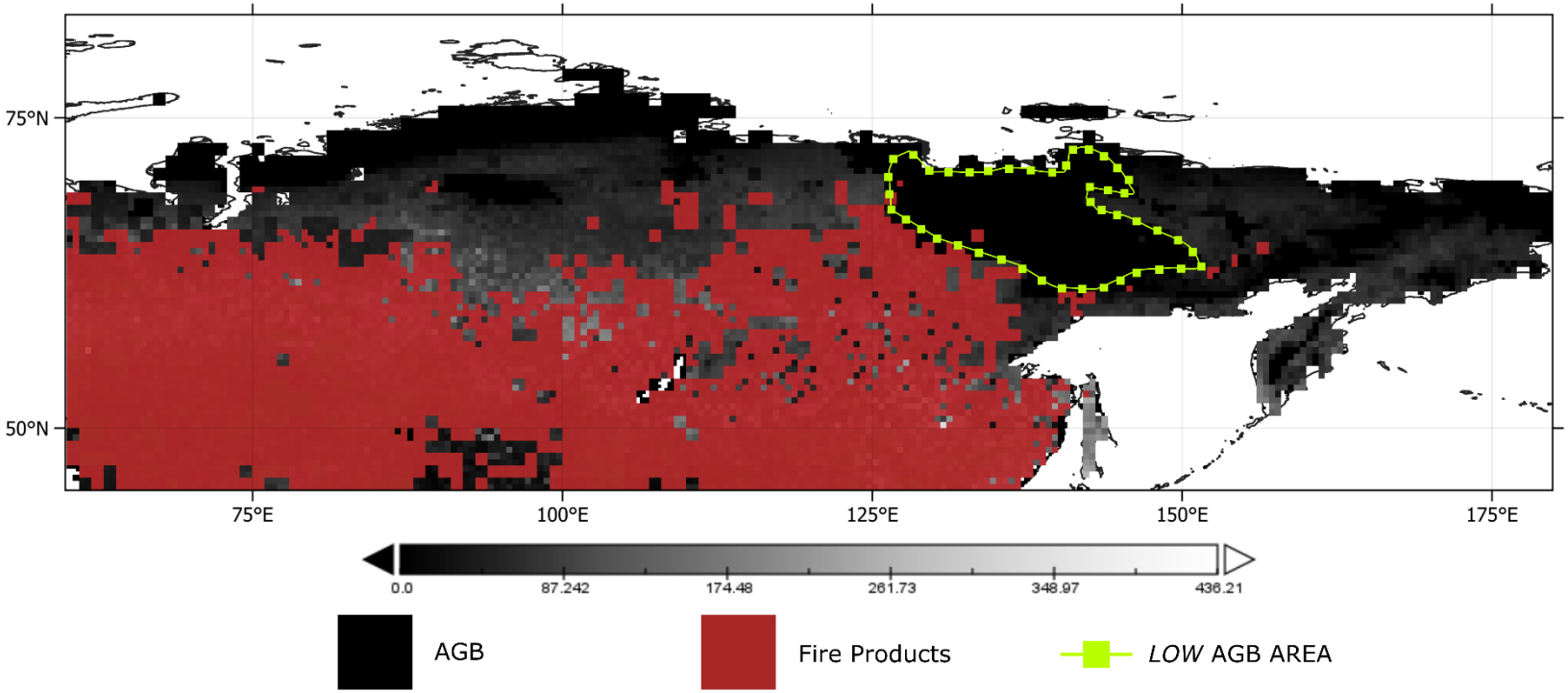

Figure S21. Spatial distribution comparison between SEIB-DGVM SPITFIRE fire products and aboveground biomass variable (1997-2016)

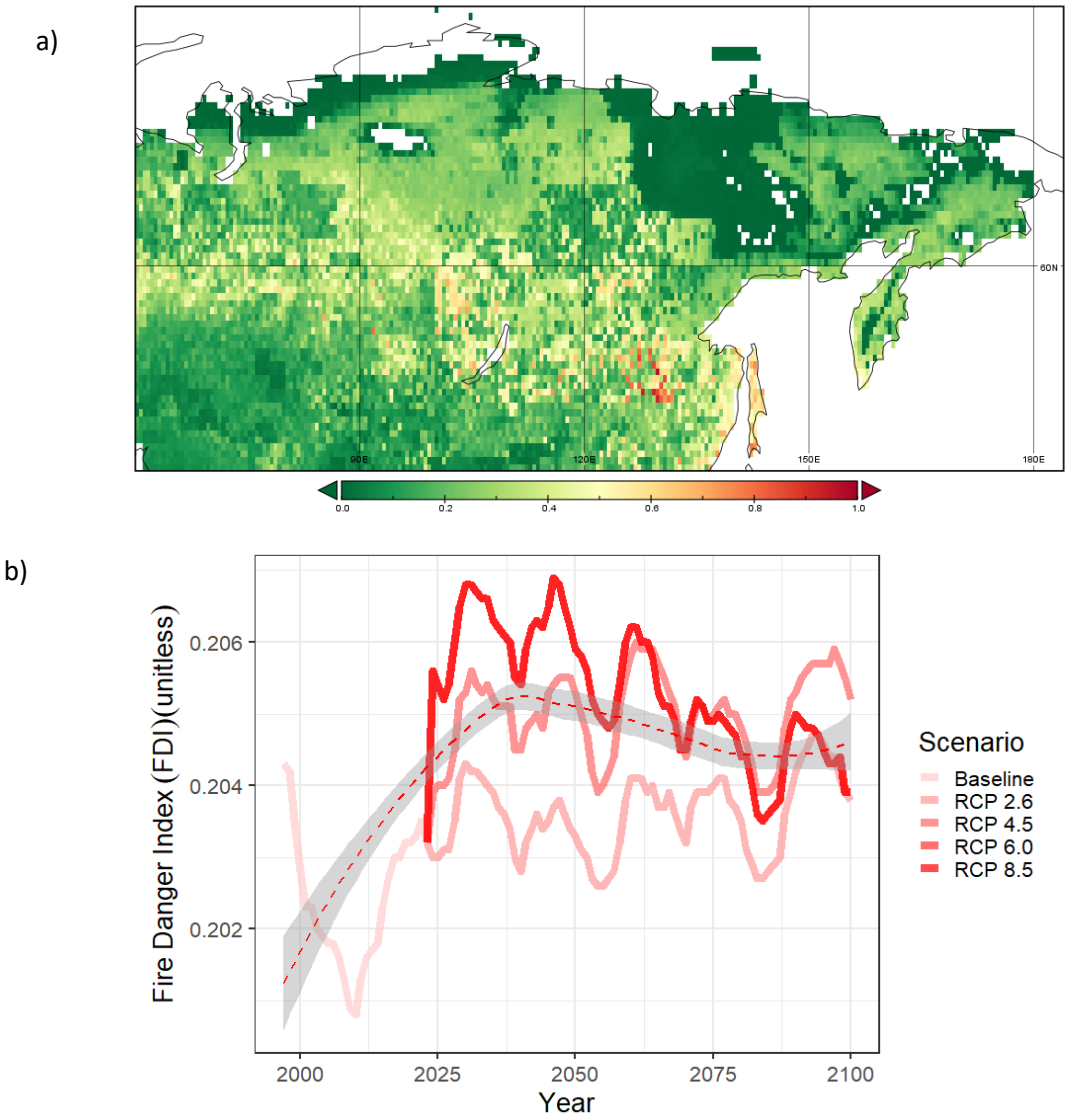

Figure S22. a) Fire Danger Index annual average map (1997-2100), b) Annual average Fire Danger Index graph

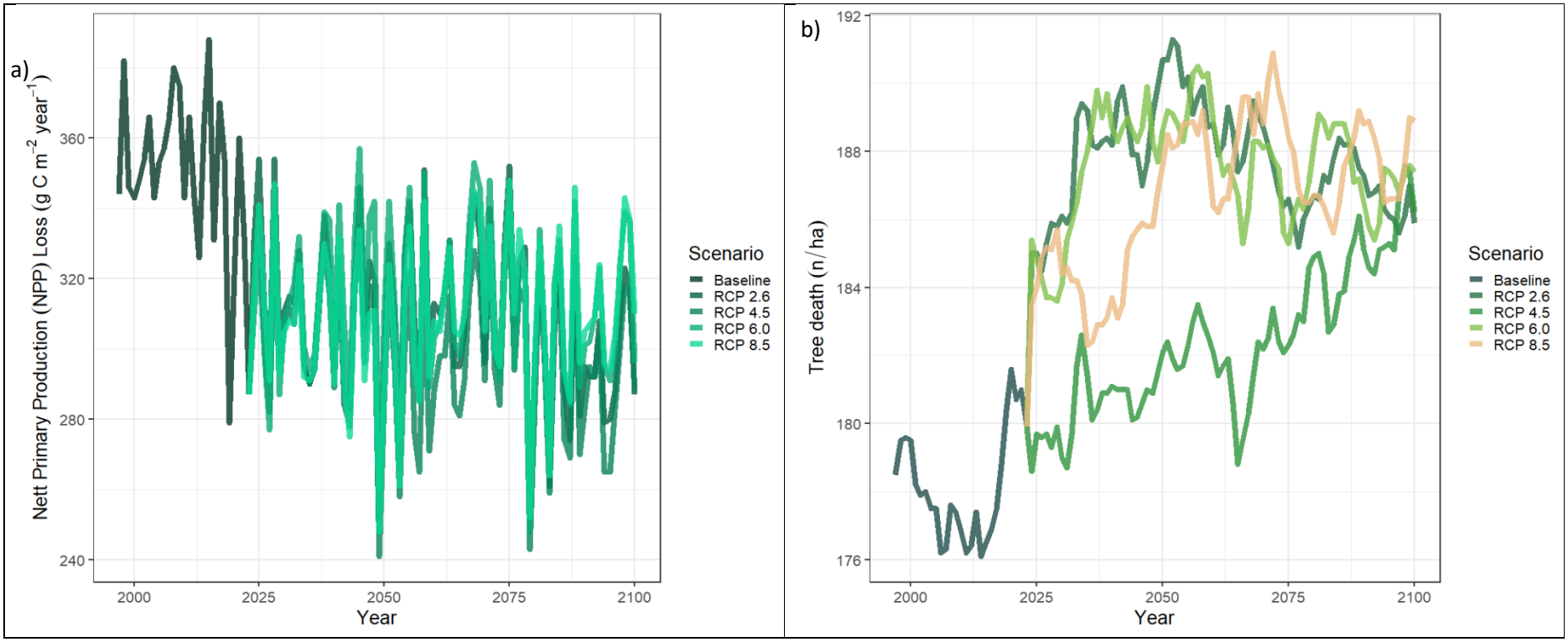

Figure S23.a) Annual average NPP loss in Siberia due to forest fires (1997-2100), b) Average number of dead trees under different climate scenarios (1997-2100)

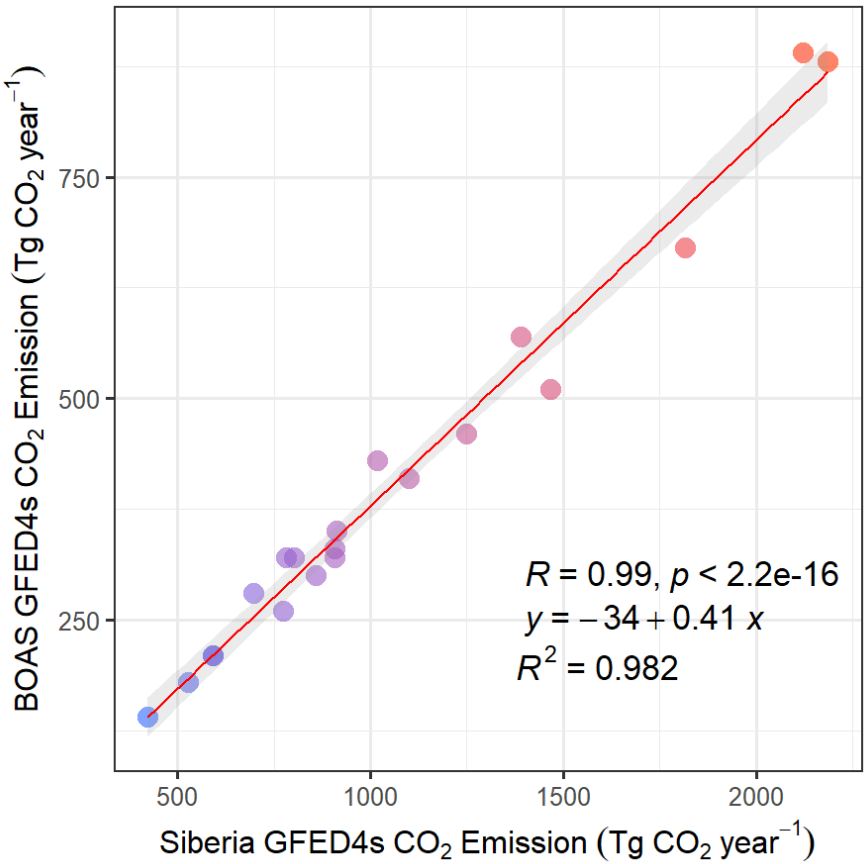

Figure S24. Annual CO2 Emissions (1997 - 2016) comparison between GFED4s research area: Siberia data extraction and GFED4s BOAS area BOAS: Boreal Asia

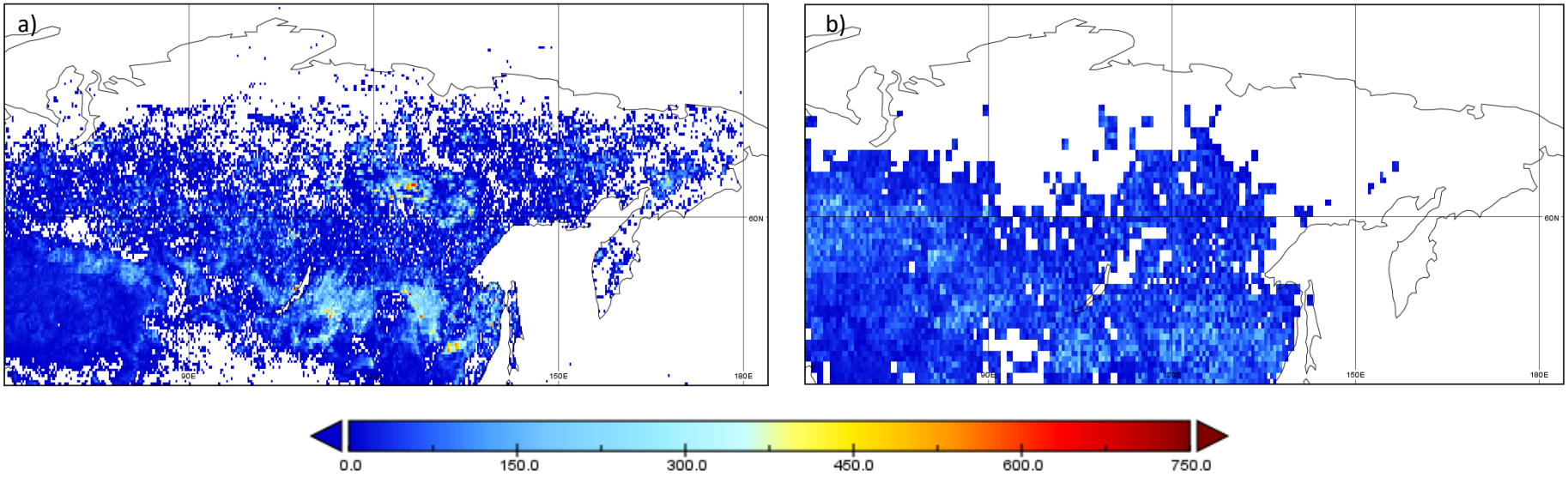

Figure S25. a) Annual average GFED4s CO_2 emissions map (1997-2016), b) Annual average SEIB-DGVM SPITFIRE CO_2 emissions map (1997-2016)

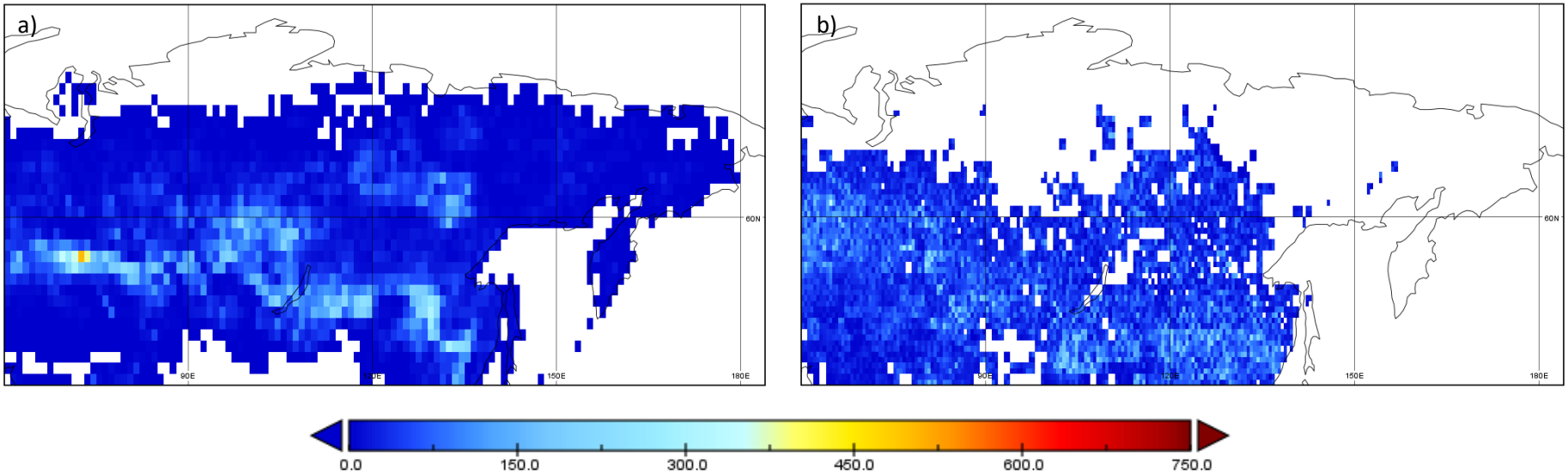

Figure S26. a) Annual average GBEI CO_2 emissions map (2001-2020), b) Annual average SEIB-DGVM SPITFIRE CO_2 emissions map (2001-2020)

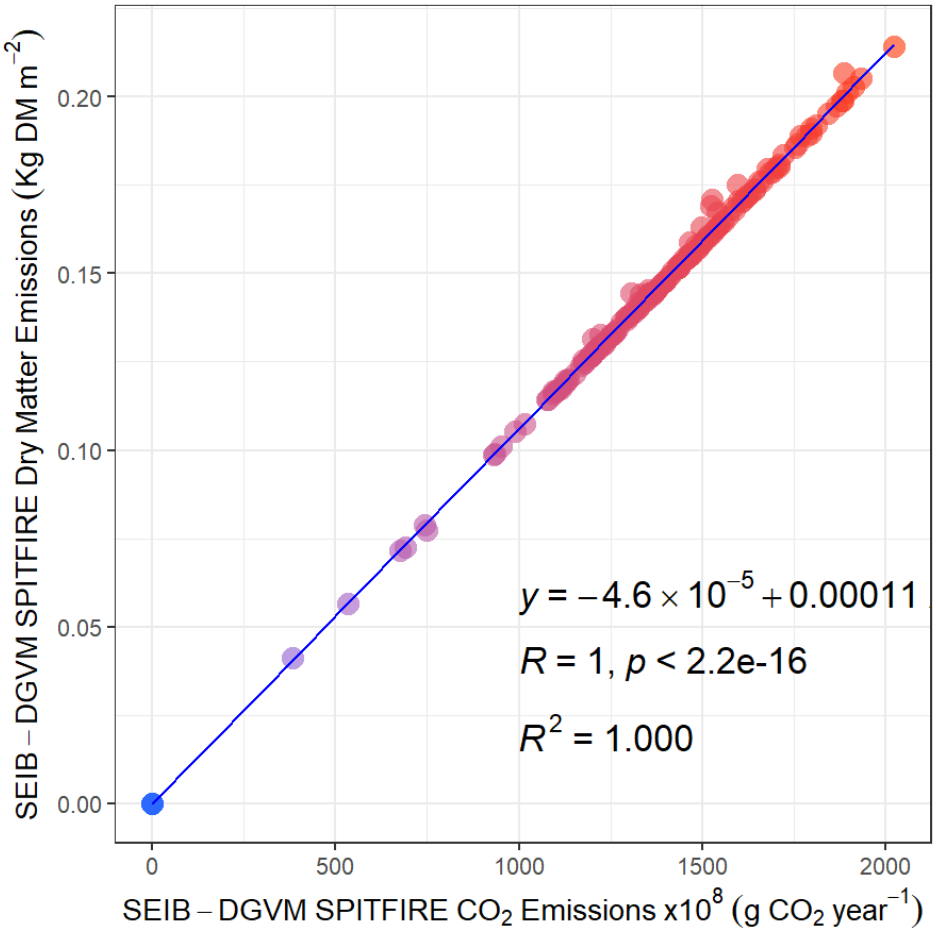

Figure S27. CO_2 and Dry Matter emissions spatial annual average (1996-2100) comparison of SEIB-DGVM SPITFIRE module product under climate baseline dataset (CRU TS.3.22)

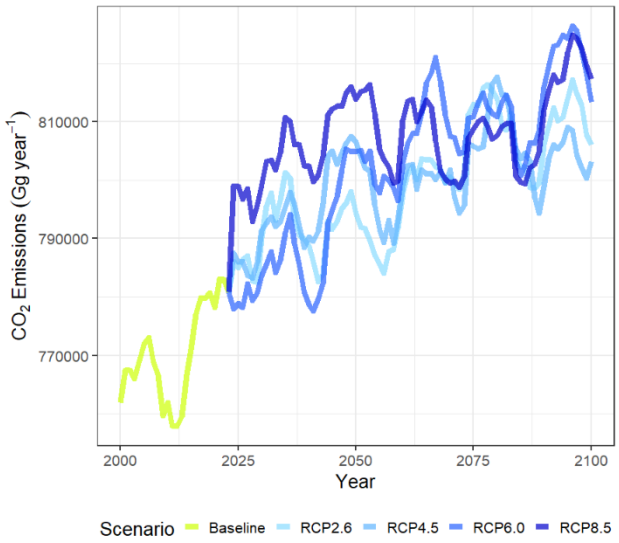
CO_2 Emissions (Gg year^{-1})
810000
790000
770000
2000
2025
2050
2075
2100
Year
Scenario
Baseline
RCP2.6
RCP4.5
RCP6.0
RCP8.5

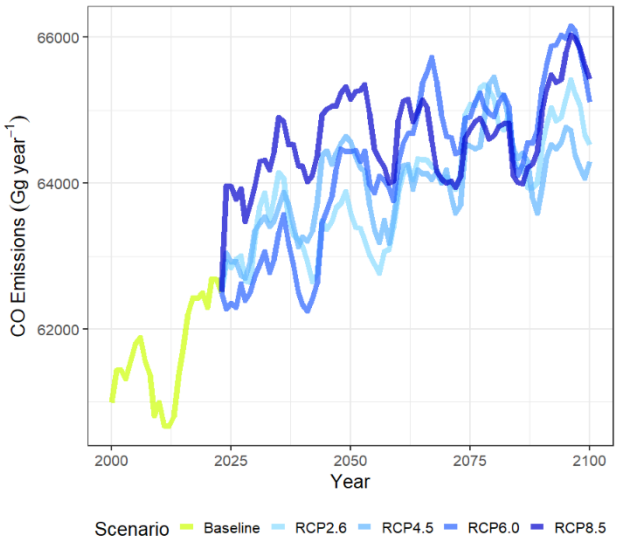
CO Emissions (Gg year^{-1})
66000
64000
62000
2000
2025
2050
2075
2100
Year
Scenario
Baseline
RCP2.6
RCP4.5
RCP6.0
RCP8.5

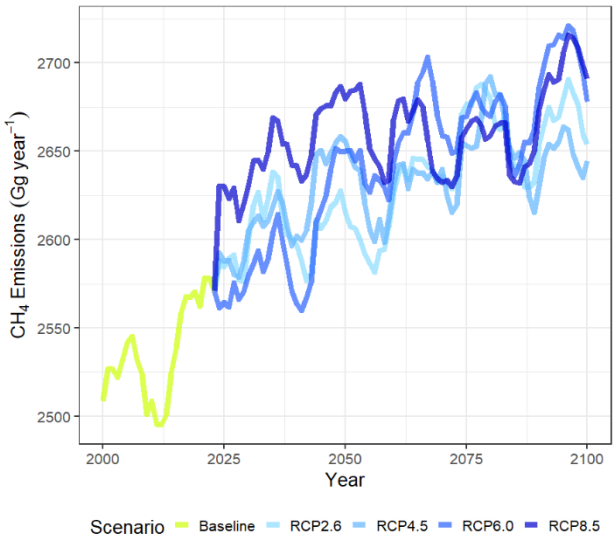
CH_4 Emissions (Gg year^{-1})
2700
2650
2600
2550
2500
2000
2025
2050
2075
2100
Year
Scenario
Baseline
RCP2.6
RCP4.5
RCP6.0
RCP8.5

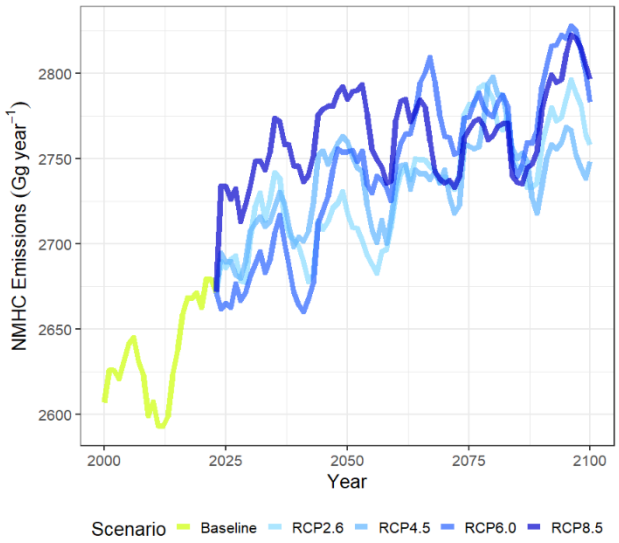
NMHC Emissions (Gg year^{-1})
2800
2750
2700
2650
2600
2000
2025
2050
2075
2100
Year
Scenario
Baseline
RCP2.6
RCP4.5
RCP6.0
RCP8.5

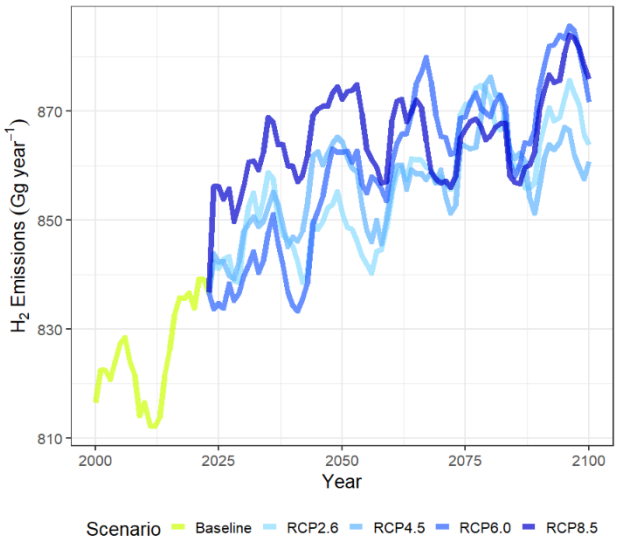
H_2 Emissions (Gg year^{-1})
870
850
830
810
2000
2025
2050
2075
2100
Year
Scenario
Baseline
RCP2.6
RCP4.5
RCP6.0
RCP8.5

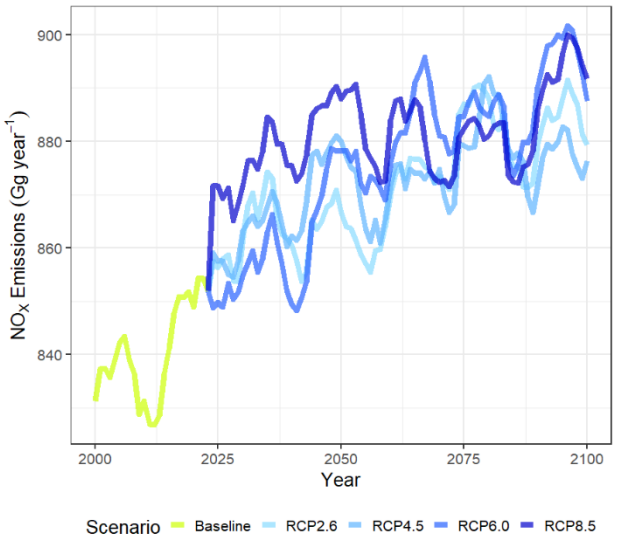
NO_X Emissions (Gg year^{-1})
900
880
860
840
2000
2025
2050
2075
2100
Year
Scenario
Baseline
RCP2.6
RCP4.5
RCP6.0
RCP8.5

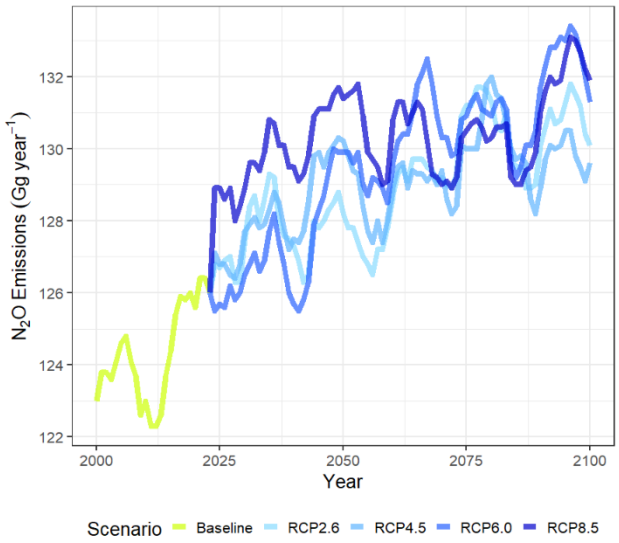
N_2O Emissions (Gg year^{-1})
132
130
128
126
124
122
2000
2025
2050
2075
2100
Year
Scenario
Baseline
RCP2.6
RCP4.5
RCP6.0
RCP8.5

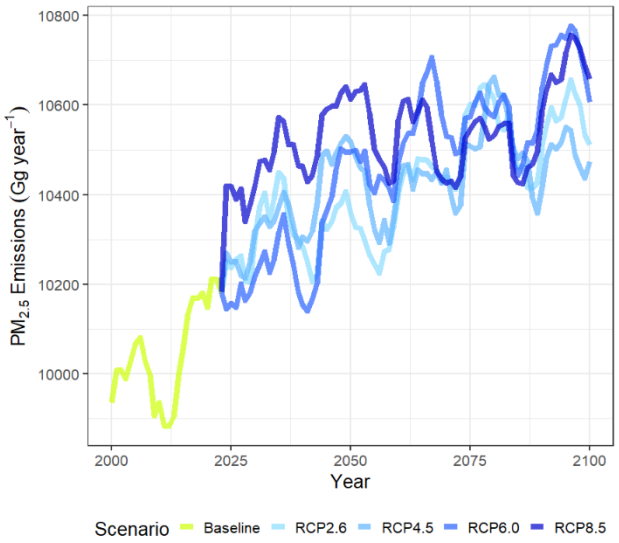
$PM_{2.5}$ Emissions (Gg year^{-1})
10800
10600
10400
10200
10000
2000
2025
2050
2075
2100
Year
Scenario
Baseline
RCP2.6
RCP4.5
RCP6.0
RCP8.5

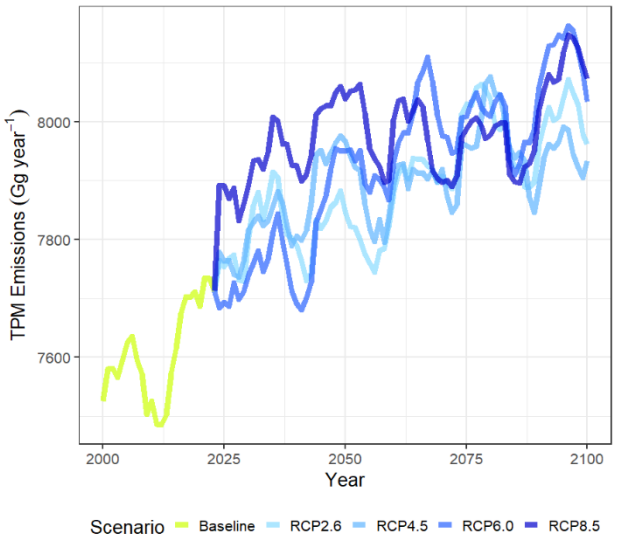
TPM Emissions (Gg year^{-1})
8000
7800
7600
2000
2025
2050
2075
2100
Year
Scenario
Baseline
RCP2.6
RCP4.5
RCP6.0
RCP8.5

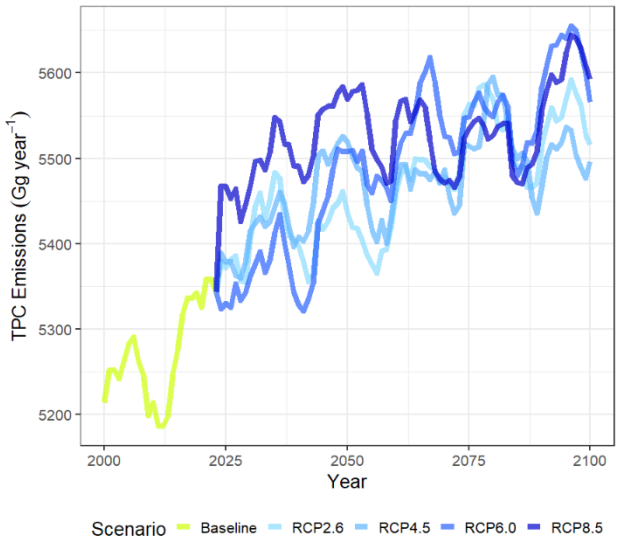
TPC Emissions (Gg year^{-1})
5600
5500
5400
5300
5200
2000
2025
2050
2075
2100
Year
Scenario
Baseline
RCP2.6
RCP4.5
RCP6.0
RCP8.5

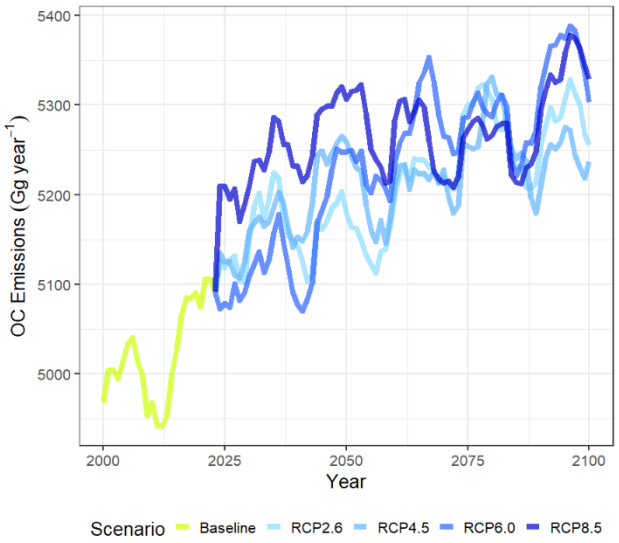
OC Emissions (Gg year^{-1})
5400
5300
5200
5100
5000
2000
2025
2050
2075
2100
Year
Scenario
Baseline
RCP2.6
RCP4.5
RCP6.0
RCP8.5

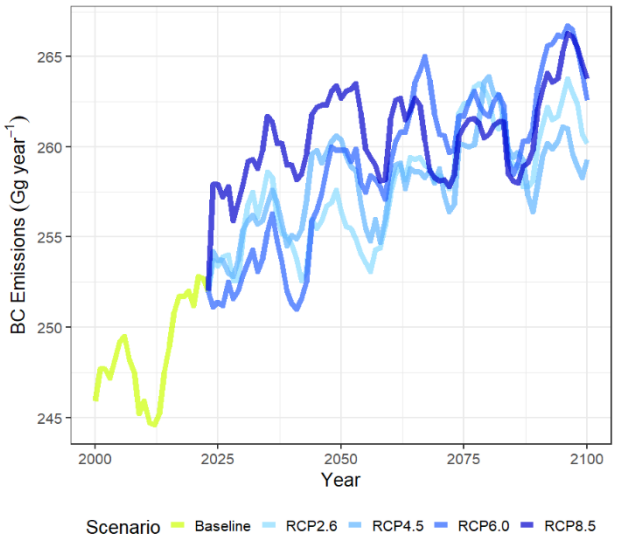
BC Emissions (Gg year^{-1})
265
260
255
250
245
2000
2025
2050
2075
2100
Year
Scenario
Baseline
RCP2.6
RCP4.5
RCP6.0
RCP8.5

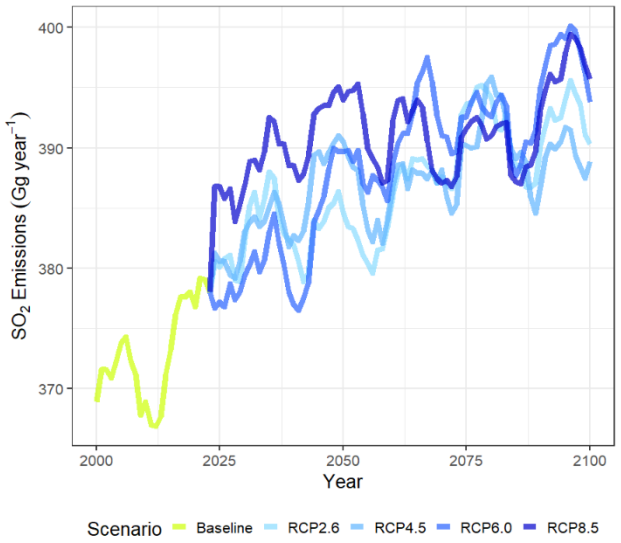
400
390
380
370
SO_2 Emissions (Gg year^{-1})
2000
2025
2050
2075
2100
Year
Scenario
Baseline
RCP2.6
RCP4.5
RCP6.0
RCP8.5

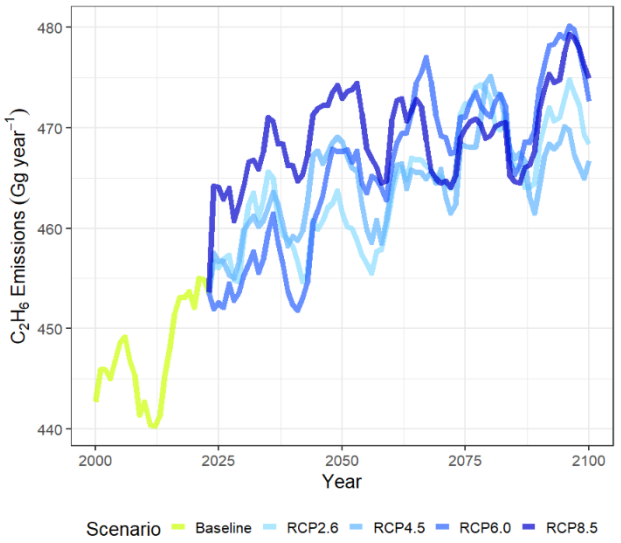
480
470
460
450
440
C_2H_6 Emissions (Gg year^{-1})
2000
2025
2050
2075
2100
Year
Scenario
Baseline
RCP2.6
RCP4.5
RCP6.0
RCP8.5

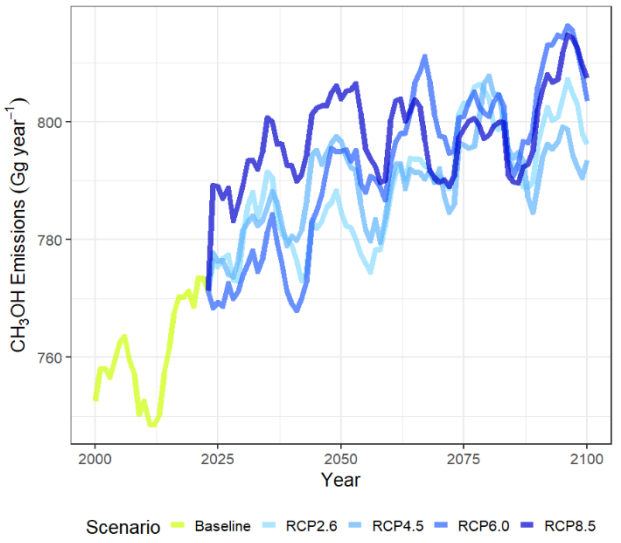
800
780
760
CH_3OH Emissions (Gg year^{-1})
2000
2025
2050
2075
2100
Year
Scenario
Baseline
RCP2.6
RCP4.5
RCP6.0
RCP8.5

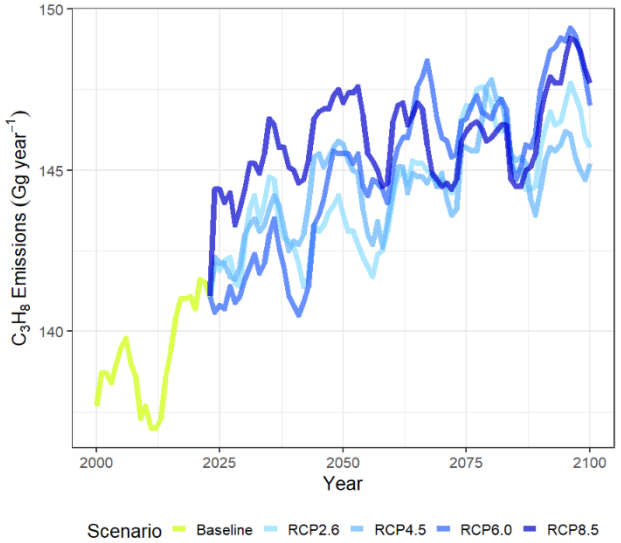
150
145
140
C_3H_8 Emissions (Gg year^{-1})
2000
2025
2050
2075
2100
Year
Scenario
Baseline
RCP2.6
RCP4.5
RCP6.0
RCP8.5

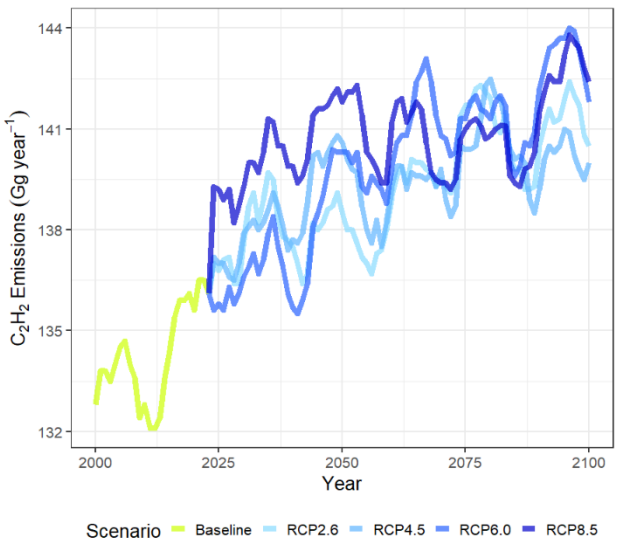
144
141
138
135
132
C_2H_2 Emissions (Gg year^{-1})
2000
2025
2050
2075
2100
Year
Scenario
Baseline
RCP2.6
RCP4.5
RCP6.0
RCP8.5

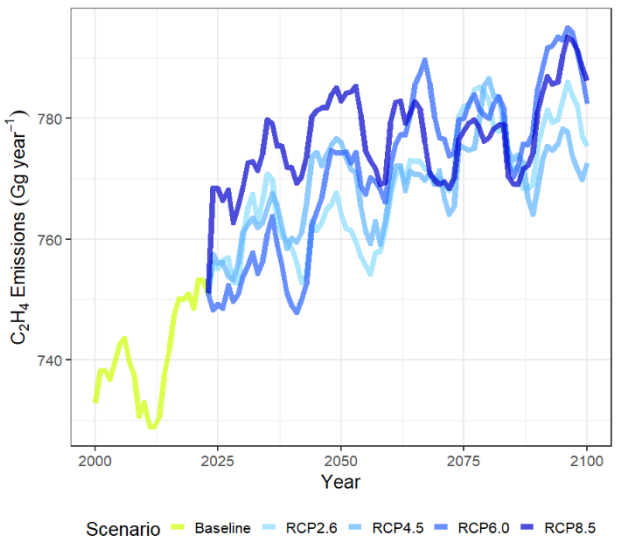
780
760
740
C_2H_4 Emissions (Gg year^{-1})
2000
2025
2050
2075
2100
Year
Scenario
Baseline
RCP2.6
RCP4.5
RCP6.0
RCP8.5

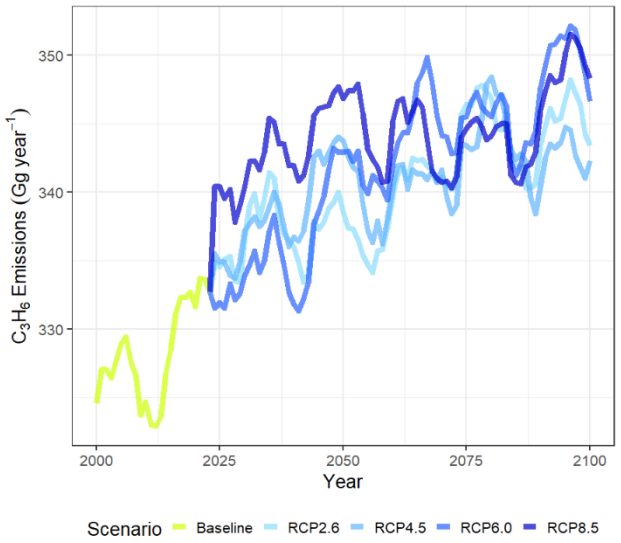
C_3H_6 Emissions (Gg year^{-1})
350
340
330
2000
2025
2050
2075
2100
Year
Scenario
Baseline
RCP2.6
RCP4.5
RCP6.0
RCP8.5

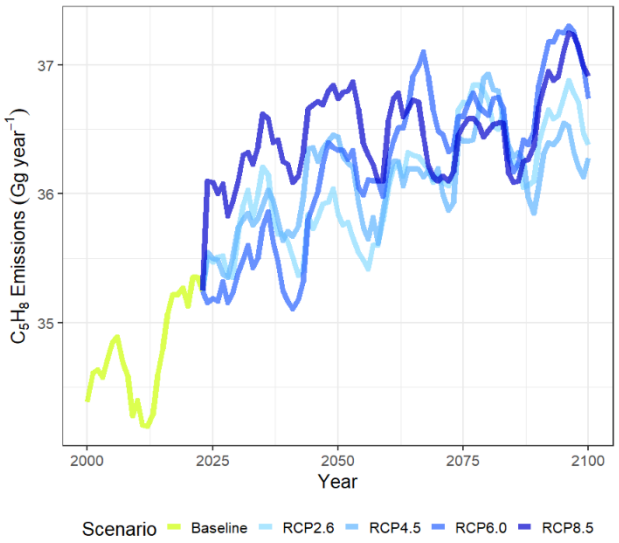
C_5H_8 Emissions (Gg year^{-1})
37
36
35
2000
2025
2050
2075
2100
Year
Scenario
Baseline
RCP2.6
RCP4.5
RCP6.0
RCP8.5

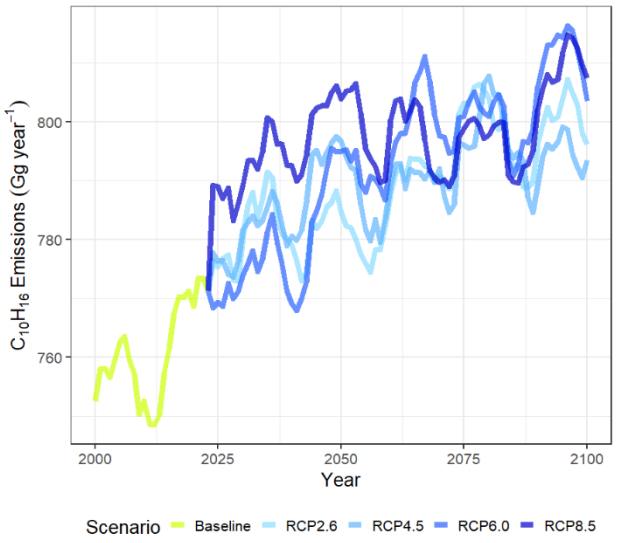
$C_{10}H_{16}$ Emissions (Gg year^{-1})
800
780
760
2000
2025
2050
2075
2100
Year
Scenario
Baseline
RCP2.6
RCP4.5
RCP6.0
RCP8.5

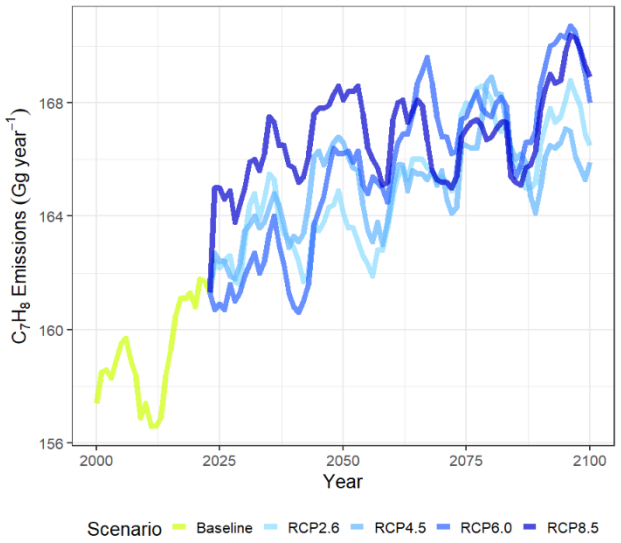
C_7H_8 Emissions (Gg year^{-1})
168
164
160
156
2000
2025
2050
2075
2100
Year
Scenario
Baseline
RCP2.6
RCP4.5
RCP6.0
RCP8.5

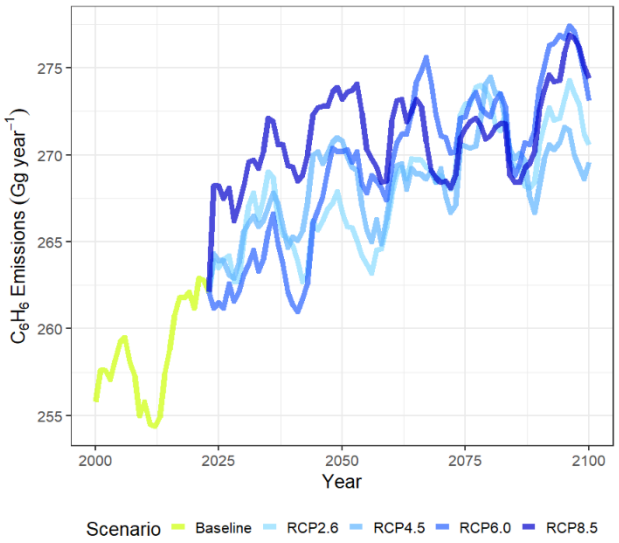
C_6H_6 Emissions (Gg year^{-1})
275
270
265
260
255
2000
2025
2050
2075
2100
Year
Scenario
Baseline
RCP2.6
RCP4.5
RCP6.0
RCP8.5

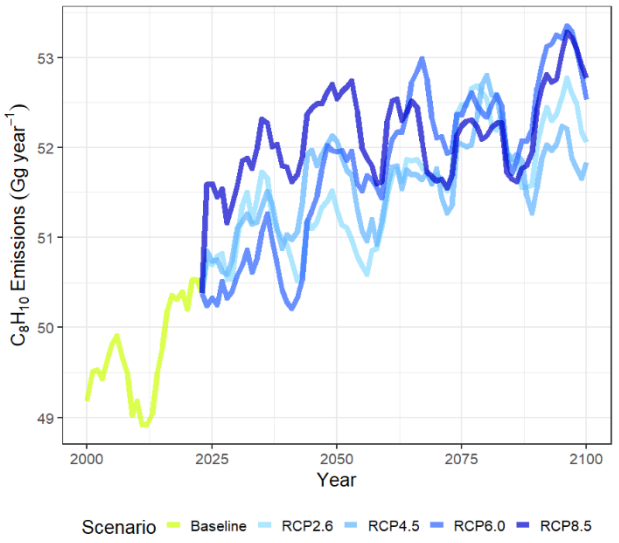
C_8H_{10} Emissions (Gg year^{-1})
53
52
51
50
49
2000
2025
2050
2075
2100
Year
Scenario
Baseline
RCP2.6
RCP4.5
RCP6.0
RCP8.5

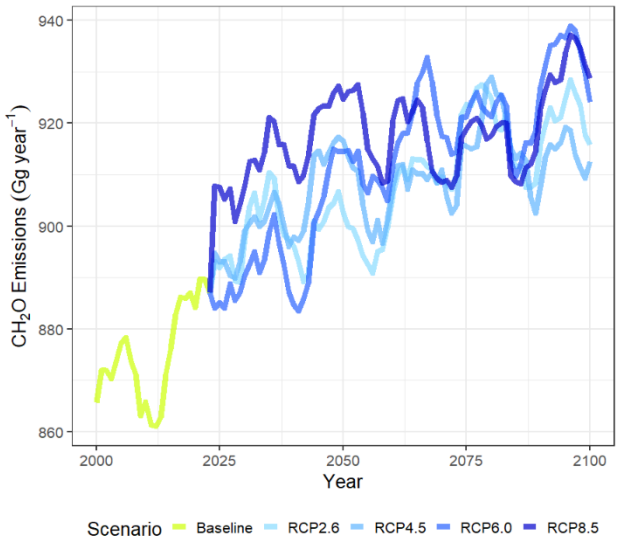
940
920
900
880
860
CH_2O Emissions (Gg year^{-1})
2000
2025
2050
2075
2100
Year
Scenario
Baseline
RCP2.6
RCP4.5
RCP6.0
RCP8.5

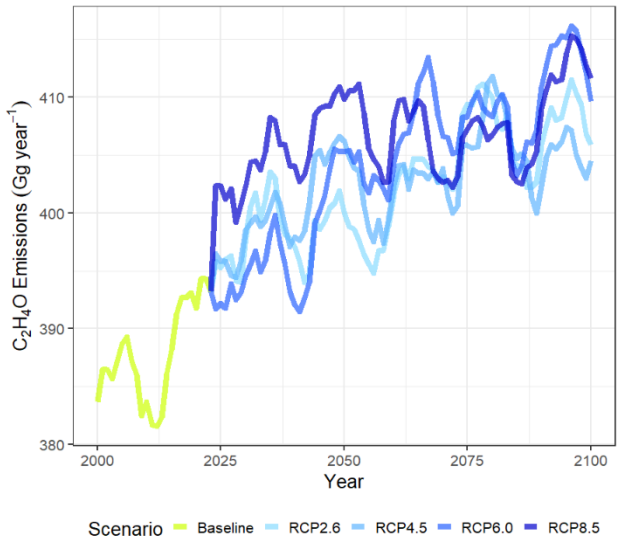
410
400
390
380
C_2H_4O Emissions (Gg year^{-1})
2000
2025
2050
2075
2100
Year
Scenario
Baseline
RCP2.6
RCP4.5
RCP6.0
RCP8.5

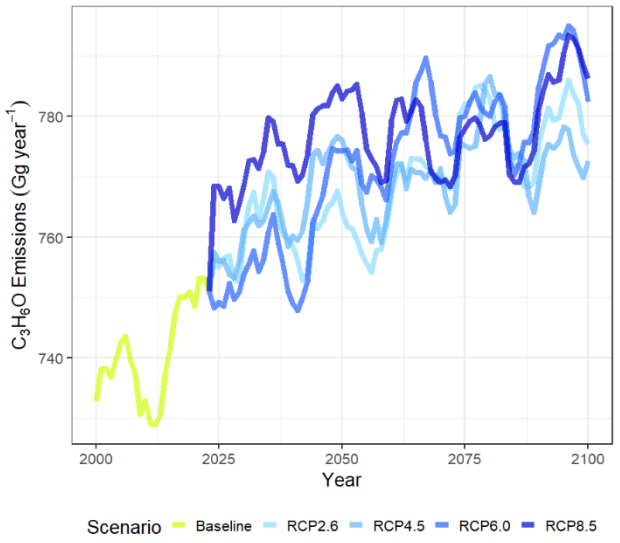
780
760
740
C_3H_6O Emissions (Gg year^{-1})
2000
2025
2050
2075
2100
Year
Scenario
Baseline
RCP2.6
RCP4.5
RCP6.0
RCP8.5

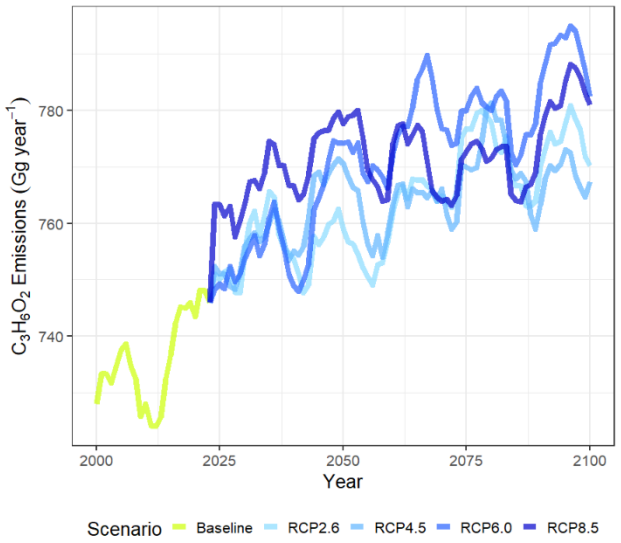
780
760
740
$C_3H_6O_2$ Emissions (Gg year^{-1})
2000
2025
2050
2075
2100
Year
Scenario
Baseline
RCP2.6
RCP4.5
RCP6.0
RCP8.5

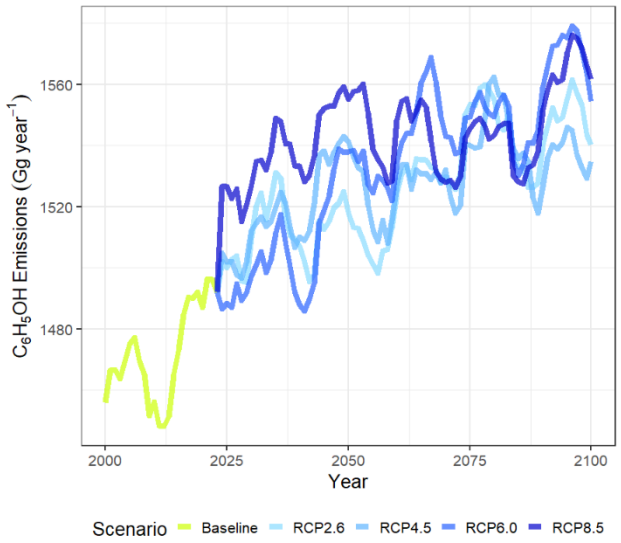
1560
1520
1480
C_6H_5OH Emissions (Gg year^{-1})
2000
2025
2050
2075
2100
Year
Scenario
Baseline
RCP2.6
RCP4.5
RCP6.0
RCP8.5

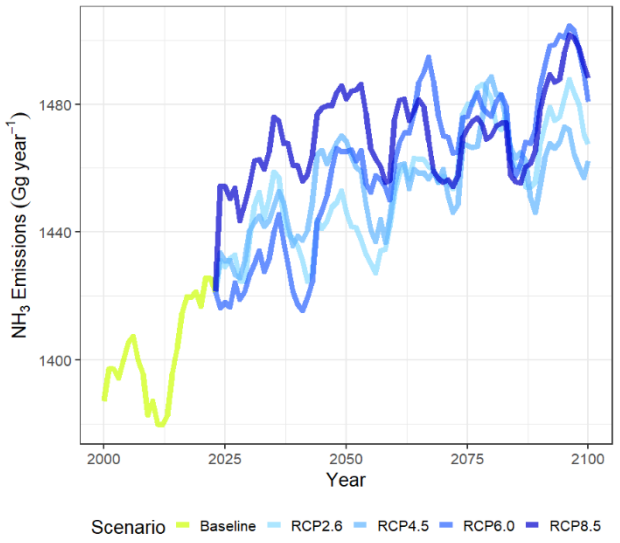
1480
1440
1400
NH_3 Emissions (Gg year^{-1})
2000
2025
2050
2075
2100
Year
Scenario
Baseline
RCP2.6
RCP4.5
RCP6.0
RCP8.5

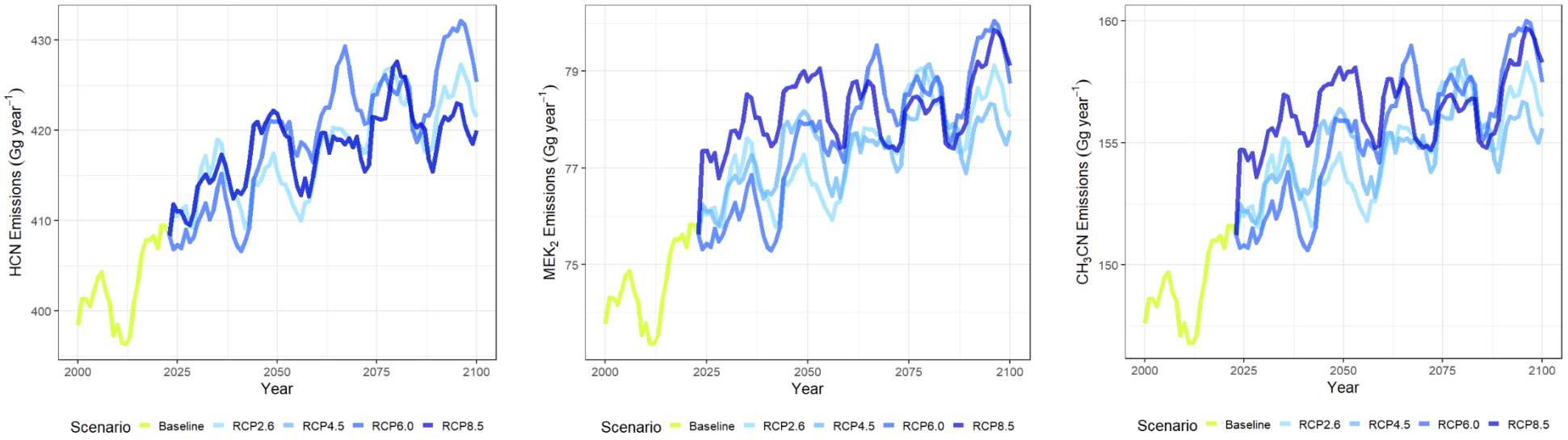

Figure S28. Projected annual emissions of 33 gaseous species from forest fires in Siberia (2023-2100)

Table S4. Projected emissions of 28 gaseous species from forest fires in Siberia (2023-2100)

sp.	Year	2000 - 2020	2021 - 2040	2041 - 2060	2061 - 2080	2081 - 2100
Gg CH_4 $year^{-1}$	**Baseline**	2530.938 ± 24.4	n.a	n.a	n.a	n.a
	RCP85	2628.648 ± 20.2	2638.610 ± 15.2	2663.170 ± 20.4	2657.595 ± 17.2	2674.775 ± 28.2
	RCP60	2622.110 ± 24.9	2581.870 ± 15.1	2625.695 ± 27.9	2671.290 ± 14.9	2684.130 ± 27.6
	RCP45	2610.776 ± 12.5	2603.640 ± 13.8	2629.405 ± 21.5	2644.755 ± 20.0	2649.680 ± 16.8
	RCP26	2620.300 ± 13.5	2604.845 ± 17.8	2602.560 ± 15.2	2653.020 ± 21.3	2659.665 ± 18.0
Gg NMHC $year^{-1}$	**Baseline**	2630.176 ± 25.3	n.a	n.a	n.a	n.a
	RCP85	2731.719 ± 20.9	2742.100 ± 15.8	2767.605 ± 21.2	2761.810 ± 17.9	2779.660 ± 29.3
	RCP60	2724.929 ± 25.9	2683.130 ± 15.7	2728.665 ± 29.0	2776.025 ± 15.5	2789.390 ± 28.7
	RCP45	2713.157 ± 13.0	2705.750 ± 14.3	2732.515 ± 22.4	2748.475 ± 20.8	2753.590 ± 17.5
	RCP26	2723.048 ± 14.0	2706.990 ± 18.5	2704.640 ± 15.9	2757.075 ± 22.1	2763.965 ± 18.7
Gg H_2 $year^{-1}$	**Baseline**	823.786 ± 7.93	n.a	n.a	n.a	n.a
	RCP85	855.595 ± 6.56	858.845 ± 4.94	866.835 ± 6.64	865.005 ± 5.60	870.605 ± 9.19
	RCP60	853.462 ± 8.09	840.370 ± 4.91	854.635 ± 9.06	869.475 ± 4.88	873.655 ± 8.99
	RCP45	849.776 ± 4.07	847.455 ± 4.49	855.835 ± 7.00	860.840 ± 6.51	862.440 ± 5.47
	RCP26	852.871 ± 4.40	847.840 ± 5.79	847.105 ± 4.97	863.535 ± 6.94	865.690 ± 5.87
Gg NO_X $year^{-1}$	**Baseline**	838.676 ± 8.07	n.a	n.a	n.a	n.a
	RCP85	871.062 ± 6.68	874.370 ± 5.02	882.490 ± 6.75	880.645 ± 5.71	886.345 ± 9.36
	RCP60	868.890 ± 8.25	855.565 ± 4.99	870.075 ± 9.23	885.200 ± 4.96	889.445 ± 9.15
	RCP45	865.143 ± 4.14	862.760 ± 4.58	871.305 ± 7.13	876.400 ± 6.62	878.025 ± 5.56
	RCP26	868.281 ± 4.47	863.160 ± 5.89	862.415 ± 5.06	879.155 ± 7.06	881.330 ± 5.97
Gg N_2O $year^{-1}$	**Baseline**	124.052 ± 1.196	n.a	n.a	n.a	n.a
	RCP85	128.843 ± 0.985	129.330 ± 0.737	130.540 ± 0.992	130.250 ± 0.837	131.085 ± 1.385
	RCP60	128.524 ± 1.228	126.560 ± 0.750	128.705 ± 1.364	130.945 ± 0.729	131.555 ± 1.359
	RCP45	127.971 ± 0.617	127.600 ± 0.682	128.880 ± 1.055	129.635 ± 0.990	129.865 ± 0.824
	RCP26	128.443 ± 0.658	127.675 ± 0.875	127.575 ± 0.752	130.050 ± 1.032	130.360 ± 0.874

sp.	Year	2000 - 2020	2021 - 2040	2041 - 2060	2061 - 2080	2081 - 2100
Gg OC $year^{-1}$	**Baseline**	5012.238 ± 48.3	n.a	n.a	n.a	n.a
	RCP85	5205.729 ± 39.9	5225.510 ± 30.0	5274.115 ± 40.4	5263.065 ± 34.1	5297.095 ± 55.9
	RCP60	5192.810 ± 49.3	5113.120 ± 29.9	5199.905 ± 55.2	5290.175 ± 29.6	5315.645 ± 54.7
	RCP45	5170.376 ± 24.8	5156.230 ± 27.4	5207.245 ± 42.6	5237.670 ± 39.7	5247.405 ± 33.2
	RCP26	5189.219 ± 26.8	5158.595 ± 35.2	5154.085 ± 30.2	5254.055 ± 42.2	5267.175 ± 35.7
Gg BC $year^{-1}$	**Baseline**	248.119 ± 2.39	n.a	n.a	n.a	n.a
	RCP85	257.710 ± 1.97	258.680 ± 1.48	261.100 ± 1.99	260.550 ± 1.70	262.240 ± 2.78
	RCP60	257.062 ± 2.45	253.120 ± 1.48	257.415 ± 2.74	261.890 ± 1.46	263.145 ± 2.70
	RCP45	255.957 ± 1.22	255.260 ± 1.36	257.785 ± 2.11	259.280 ± 1.97	259.765 ± 1.64
	RCP26	256.886 ± 1.32	255.380 ± 1.74	255.150 ± 1.48	260.095 ± 2.09	260.750 ± 1.77
Gg SO_2 $year^{-1}$	**Baseline**	372.186 ± 3.59	n.a	n.a	n.a	n.a
	RCP85	386.557 ± 2.98	388.035 ± 2.23	391.645 ± 2.99	390.825 ± 2.53	393.345 ± 4.16
	RCP60	385.595 ± 3.66	379.680 ± 2.21	386.140 ± 4.10	392.830 ± 2.19	394.715 ± 4.06
	RCP45	383.924 ± 1.83	382.885 ± 2.01	386.675 ± 3.17	388.935 ± 2.93	389.655 ± 2.47
	RCP26	385.333 ± 1.99	383.075 ± 2.62	382.725 ± 2.24	390.150 ± 3.13	391.120 ± 2.64
Gg C_2H_6 $year^{-1}$	**Baseline**	446.633 ± 4.31	n.a	n.a	n.a	n.a
	RCP85	463.881 ± 3.55	465.630 ± 2.68	469.975 ± 3.61	468.985 ± 3.04	472.005 ± 4.99
	RCP60	462.724 ± 4.39	455.620 ± 2.67	463.355 ± 4.90	471.390 ± 2.63	473.680 ± 4.87
	RCP45	460.719 ± 2.20	459.455 ± 2.43	463.995 ± 3.80	466.720 ± 3.53	467.590 ± 2.96
	RCP26	462.405 ± 2.39	459.675 ± 3.14	459.270 ± 2.70	468.185 ± 3.77	469.340 ± 3.18
Gg CH_3OH $year^{-1}$	**Baseline**	759.281 ± 7.31	n.a	n.a	n.a	n.a
	RCP85	788.576 ± 6.05	791.570 ± 4.53	798.945 ± 6.13	797.275 ± 5.15	802.430 ± 8.47
	RCP60	786.633 ± 7.48	774.560 ± 4.52	787.695 ± 8.36	801.375 ± 4.49	805.240 ± 8.28
	RCP45	783.229 ± 3.76	781.085 ± 4.15	788.815 ± 6.45	793.430 ± 6.01	794.895 ± 5.03
	RCP26	786.081 ± 4.05	781.450 ± 5.34	780.770 ± 4.56	795.910 ± 6.41	797.900 ± 5.41

sp.	Year	2000 - 2020	2021 - 2040	2041 - 2060	2061 - 2080	2081 - 2100
Gg C_3H_8 year^{-1}	**Baseline**	138.948 ± 1.347	n.a	n.a	n.a	n.a
	RCP85	144.300 ± 1.103	144.850 ± 0.851	146.210 ± 1.129	145.900 ± 0.936	146.840 ± 1.552
	RCP60	143.948 ± 1.368	141.750 ± 0.822	144.150 ± 1.542	146.640 ± 0.816	147.350 ± 1.516
	RCP45	143.329 ± 0.682	142.935 ± 0.758	144.345 ± 1.181	145.195 ± 1.101	145.465 ± 0.903
	RCP26	143.852 ± 0.744	143.005 ± 0.971	142.870 ± 0.839	145.645 ± 1.182	146.010 ± 0.984
Gg C_2H_2 year^{-1}	**Baseline**	133.971 ± 1.283	n.a	n.a	n.a	n.a
	RCP85	139.157 ± 1.063	139.695 ± 0.802	140.975 ± 1.075	140.695 ± 0.916	141.585 ± 1.488
	RCP60	138.814 ± 1.315	136.680 ± 0.802	139.000 ± 1.476	141.420 ± 0.796	142.095 ± 1.449
	RCP45	138.210 ± 0.664	137.815 ± 0.730	139.210 ± 1.151	140.005 ± 1.063	140.260 ± 0.881
	RCP26	138.710 ± 0.717	137.900 ± 0.951	137.780 ± 0.795	140.430 ± 1.149	140.795 ± 0.968
Gg C_2H_4 year^{-1}	**Baseline**	739.429 ± 7.12	n.a	n.a	n.a	n.a
	RCP85	767.981 ± 5.89	770.880 ± 4.43	778.065 ± 5.97	776.430 ± 5.02	781.445 ± 8.23
	RCP60	766.067 ± 7.27	754.300 ± 4.41	767.120 ± 8.15	780.430 ± 4.35	784.180 ± 8.05
	RCP45	762.748 ± 3.66	760.660 ± 4.04	768.200 ± 6.29	772.690 ± 5.85	774.120 ± 4.90
	RCP26	765.529 ± 3.95	761.015 ± 5.20	760.360 ± 4.46	775.110 ± 6.22	777.040 ± 5.26
Gg C_3H_6 year^{-1}	**Baseline**	327.538 ± 3.16	n.a	n.a	n.a	n.a
	RCP85	340.176 ± 2.60	341.460 ± 1.97	344.645 ± 2.64	343.915 ± 2.23	346.145 ± 3.66
	RCP60	339.319 ± 3.23	334.125 ± 1.96	339.795 ± 3.60	345.705 ± 1.92	347.355 ± 3.58
	RCP45	337.857 ± 1.60	336.935 ± 1.79	340.275 ± 2.80	342.245 ± 2.60	342.900 ± 2.17
	RCP26	339.105 ± 1.74	337.090 ± 2.31	336.795 ± 1.98	343.335 ± 2.75	344.180 ± 2.35
Gg C_5H_8 year^{-1}	**Baseline**	34.698 ± 0.341	n.a	n.a	n.a	n.a
	RCP85	36.055 ± 0.283	36.202 ± 0.209	36.525 ± 0.282	36.459 ± 0.232	36.688 ± 0.385
	RCP60	35.968 ± 0.333	35.417 ± 0.208	36.011 ± 0.387	36.645 ± 0.208	36.813 ± 0.382
	RCP45	35.792 ± 0.175	35.712 ± 0.191	36.074 ± 0.296	36.284 ± 0.282	36.342 ± 0.241
	RCP26	35.934 ± 0.185	35.733 ± 0.242	35.707 ± 0.206	36.388 ± 0.287	36.468 ± 0.245

sp.	Year	2000 - 2020	2021 - 2040	2041 - 2060	2061 - 2080	2081 - 2100
Gg $C_{10}H_{16}$ year^{-1}	**Baseline**	759.281 ± 7.31	n.a	n.a	n.a	n.a
	RCP85	788.576 ± 6.05	791.570 ± 4.53	798.945 ± 6.13	797.275 ± 5.15	802.430 ± 8.47
	RCP60	786.633 ± 7.48	774.560 ± 4.52	787.695 ± 8.36	801.375 ± 4.49	805.240 ± 8.28
	RCP45	783.229 ± 3.76	781.085 ± 4.15	788.815 ± 6.45	793.430 ± 6.01	794.895 ± 5.03
	RCP26	786.081 ± 4.05	781.450 ± 5.34	780.770 ± 4.56	795.910 ± 6.41	797.900 ± 5.41
Gg C_7H_8 year^{-1}	**Baseline**	158.814 ± 1.530	n.a	n.a	n.a	n.a
	RCP85	164.929 ± 1.257	165.540 ± 0.953	167.080 ± 1.283	166.740 ± 1.074	167.825 ± 1.778
	RCP60	164.514 ± 1.564	161.985 ± 0.945	164.725 ± 1.753	167.595 ± 0.932	168.405 ± 1.732
	RCP45	163.819 ± 0.788	163.360 ± 0.859	164.965 ± 1.357	165.925 ± 1.265	166.245 ± 1.056
	RCP26	164.405 ± 0.850	163.430 ± 1.117	163.295 ± 0.952	166.450 ± 1.330	166.865 ± 1.121
Gg C_6H_6 year^{-1}	**Baseline**	258.043 ± 2.49	n.a	n.a	n.a	n.a
	RCP85	268.005 ± 2.05	269.030 ± 1.54	271.535 ± 2.08	270.965 ± 1.75	272.715 ± 2.88
	RCP60	267.352 ± 2.53	263.260 ± 1.55	267.710 ± 2.85	272.365 ± 1.53	273.680 ± 2.82
	RCP45	266.181 ± 1.28	265.460 ± 1.41	268.100 ± 2.19	269.665 ± 2.04	270.160 ± 1.71
	RCP26	267.176 ± 1.37	265.590 ± 1.82	265.355 ± 1.55	270.495 ± 2.17	271.175 ± 1.83
Gg C_8H_{10} year^{-1}	**Baseline**	49.617 ± 0.478	n.a	n.a	n.a	n.a
	RCP85	51.539 ± 0.390	51.736 ± 0.296	52.224 ± 0.410	52.108 ± 0.334	52.451 ± 0.555
	RCP60	51.413 ± 0.490	50.632 ± 0.290	51.489 ± 0.545	52.382 ± 0.292	52.635 ± 0.534
	RCP45	51.190 ± 0.250	51.054 ± 0.265	51.539 ± 0.424	51.853 ± 0.399	51.943 ± 0.330
	RCP26	51.381 ± 0.255	51.077 ± 0.342	51.023 ± 0.305	52.010 ± 0.419	52.157 ± 0.356
Gg CH_2O year^{-1}	**Baseline**	873.424 ± 8.42	n.a	n.a	n.a	n.a
	RCP85	907.133 ± 6.95	910.575 ± 5.23	919.050 ± 7.04	917.140 ± 5.93	923.055 ± 9.74
	RCP60	904.886 ± 8.60	891.000 ± 5.20	906.125 ± 9.61	921.855 ± 5.16	926.285 ± 9.53
	RCP45	900.967 ± 4.31	898.510 ± 4.76	907.405 ± 7.42	912.690 ± 6.90	914.395 ± 5.79

sp.	Year	2000 - 2020	2021 - 2040	2041 - 2060	2061 - 2080	2081 - 2100
	RCP26	904.262 ± 4.65	898.915 ± 6.15	898.130 ± 5.27	915.550 ± 7.35	917.855 ± 6.22
Gg C_2H_4O year^{-1}	**Baseline**	387.076 ± 3.73	n.a	n.a	n.a	n.a
	RCP85	402.019 ± 3.08	403.545 ± 2.32	407.300 ± 3.12	406.450 ± 2.64	409.075 ± 4.31
	RCP60	401.019 ± 3.81	394.875 ± 2.31	401.575 ± 4.26	408.535 ± 2.28	410.500 ± 4.22
	RCP45	399.295 ± 1.92	398.195 ± 2.11	402.140 ± 3.29	404.495 ± 3.08	405.240 ± 2.56
	RCP26	400.743 ± 2.07	398.375 ± 2.72	398.035 ± 2.34	405.755 ± 3.27	406.770 ± 2.77
Gg C_3H_6O year^{-1}	**Baseline**	739.429 ± 7.12	n.a	n.a	n.a	n.a
	RCP85	767.981 ± 5.89	770.880 ± 4.43	778.065 ± 5.97	776.430 ± 5.02	781.445 ± 8.23
	RCP60	766.067 ± 3.23	754.300 ± 1.96	767.120 ± 3.60	780.430 ± 1.92	784.180 ± 3.58
	RCP45	762.748 ± 3.66	760.660 ± 4.04	768.200 ± 6.29	772.690 ± 5.85	774.120 ± 4.90
	RCP26	765.529 ± 3.95	761.015 ± 5.20	760.360 ± 4.46	775.110 ± 6.22	777.040 ± 5.26
Gg $C_3H_6O_2$ year^{-1}	**Baseline**	734.462 ± 7.08	n.a	n.a	n.a	n.a
	RCP85	762.814 ± 5.85	765.720 ± 4.40	772.830 ± 5.92	771.210 ± 4.99	776.200 ± 8.19
	RCP60	766.067 ± 7.27	754.300 ± 4.41	767.120 ± 8.15	780.430 ± 4.35	784.180 ± 8.05
	RCP45	757.624 ± 3.63	755.565 ± 4.01	763.035 ± 6.25	767.515 ± 5.81	768.925 ± 4.87
	RCP26	760.386 ± 3.91	755.905 ± 5.15	755.255 ± 4.43	769.900 ± 6.20	771.825 ± 5.23
Gg C_6H_5OH year^{-1}	**Baseline**	1468.938 ± 14.16	n.a	n.a	n.a	n.a
	RCP85	1525.648 ± 11.70	1531.440 ± 8.81	1545.685 ± 11.85	1542.450 ± 9.98	1552.415 ± 16.39
	RCP60	1521.852 ± 14.45	1498.505 ± 8.76	1523.950 ± 16.16	1550.400 ± 8.69	1557.850 ± 16.02
	RCP45	1515.300 ± 7.26	1511.130 ± 8.02	1526.090 ± 12.49	1535.000 ± 11.63	1537.855 ± 9.75
	RCP26	1520.805 ± 7.84	1511.830 ± 10.33	1510.505 ± 8.87	1539.795 ± 12.36	1543.640 ± 10.47
Gg NH_3 year^{-1}	**Baseline**	1399.467 ± 13.48	n.a	n.a	n.a	n.a
	RCP85	1453.476 ± 11.15	1459.010 ± 8.39	1472.575 ± 11.28	1469.495 ± 9.52	1479.005 ± 15.60
	RCP60	1449.862 ± 13.76	1427.625 ± 8.34	1451.855 ± 15.41	1477.055 ± 8.27	1484.170 ± 15.27
	RCP45	1443.610 ± 6.90	1439.665 ± 7.65	1453.895 ± 11.89	1462.400 ± 11.07	1465.120 ± 9.29

sp.	Year	2000 - 2020	2021 - 2040	2041 - 2060	2061 - 2080	2081 - 2100
	RCP26	1448.876 ± 7.47	1440.325 ± 9.85	1439.055 ± 8.44	1466.975 ± 11.78	1470.645 ± 9.98
Gg HCN $year^{-1}$	**Baseline**	401.967 ± 3.88	n.a	n.a	n.a	n.a
	RCP85	57.791 ± 0.41	58.245 ± 0.51	58.257 ± 0.36	58.965 ± 0.38	59.015 ± 0.36
	RCP60	416.448 ± 3.95	410.060 ± 2.39	417.025 ± 4.42	424.260 ± 2.36	426.290 ± 4.38
	RCP45	414.648 ± 1.99	413.520 ± 2.20	417.600 ± 3.42	420.050 ± 3.18	420.835 ± 2.66
	RCP26	416.171 ± 2.15	413.705 ± 2.82	413.345 ± 2.42	421.365 ± 3.38	422.420 ± 2.86
Gg MEK_2 $year^{-1}$	**Baseline**	74.430 ± 0.725	n.a	n.a	n.a	n.a
	RCP85	77.310 ± 0.601	77.598 ± 0.450	78.324 ± 0.596	78.158 ± 0.504	78.667 ± 0.828
	RCP60	77.115 ± 0.734	75.925 ± 0.440	77.221 ± 0.819	78.563 ± 0.444	78.935 ± 0.824
	RCP45	76.780 ± 0.372	76.565 ± 0.407	77.320 ± 0.635	77.782 ± 0.583	77.929 ± 0.502
	RCP26	77.065 ± 0.398	76.617 ± 0.525	76.538 ± 0.447	78.029 ± 0.628	78.211 ± 0.529
Gg CH_3CN $year^{-1}$	**Baseline**	148.867 ± 1.425	n.a	n.a	n.a	n.a
	RCP85	154.610 ± 1.179	155.195 ± 0.899	156.640 ± 1.212	156.315 ± 1.012	157.325 ± 1.656
	RCP60	154.229 ± 1.469	151.865 ± 0.889	154.450 ± 1.642	157.130 ± 0.875	157.870 ± 1.613
	RCP45	153.586 ± 0.731	153.145 ± 0.806	154.650 ± 1.259	155.560 ± 1.185	155.835 ± 0.990
	RCP26	154.129 ± 0.806	153.210 ± 1.056	153.075 ± 0.908	156.060 ± 1.248	156.450 ± 1.060

Refferences

Agee, J.K. (1997) 'Fire Ecology of Pacific Northwest Forests', *Electronic Green Journal*, 1(7). Available at: https://doi.org/10.5070/g31710279.

Andreae, M. (2019) 'Emission of trace gases and aerosols from biomass burning. Global Biogeochemical', *Atomospheric Chemistry and Physics*, 15 (4)(April), pp. 955–966. Available at: https://www.atmos-chem-phys-discuss.net/acp-2019-303/acp-2019-303.pdf.

Andreae, M.O. and Merlet, P. (2001) 'Emission of trace gases and aerosols from biomass burning', 15(4), pp. 955–966.

Archibald, S., Roy, D.P., van Wilgen, B.W. and Scholes, R.J. (2009) 'What limits fire? An examination of drivers of burnt area in Southern Africa', *Global Change Biology*, 15(3), pp. 613–630. Available at: https://doi.org/10.1111/j.1365-2486.2008.01754.x.

Byram, G.M. (1959) 'Combustion of forest fuels', in K.P. Davis (ed.) *Forest Fire Control and Use*. New York: McGraw-Hill, pp. 61–89. Available at: https://doi.org/10.2307/1932261.

Cecil and Daniel, J. (2001) 'LIS/OTD 0.5 Degree High Resolution Full Climatology (HRFC) V2.3.2015'. NASA Global Hydrometeorology Resource Center DAAC, Huntsville, Alabama, U.S.A. Available at: https://doi.org/http://dx.doi.org/10.5067/LIS/LIS-OTD/DATA302.

CIESIN (2018) 'Gridded Population of the World, Version 4.11 (GPWv4): Population Count, Revision 11', *Revision 11. Palisades, NY: NASA Socioeconomic Data and Applications Center (SEDAC)* [Preprint]. Palisades, NY: NASA Socioeconomic Data and Applications Center (SEDAC). Available at: https://doi.org/https://doi.org/10.7927/H4JW8BX5.

Cochrane, M.A. (2003) 'Fire science for rainforests', *Nature*, 421(6926), pp. 913–919. Available at: https://doi.org/10.1038/nature01437.

Dickinson, M.B. and Johnson, E.A. (2001) 'Fire Effects on Trees', in *Forest Fires*, pp. 477–525. Available at: https://doi.org/10.1016/b978-012386660-8/50016-7.

Hessilt, T.D., Werf, G. Van Der, Abatzoglou, J.T. and Scholten, R.C. (2021) 'Future increases in lightning-ignited boreal fires from conjunct increases in dry fuels and lightning', *Proceedings of the 23rd EGU General Assembly* [Preprint].

Ivanova, G.A. and Ivanov, V.A. (2005) 'Fire Regimes in Siberian Forests', *International Forest Fire News (IFFN)*, 32(1), pp. 67–69.

Jones, P.W. (1999) 'First- and second-order conservative remapping schemes for grids in spherical coordinates', *Monthly Weather Review*, 127(9), pp. 2204–2210. Available at: https://doi.org/10.1175/1520-0493(1999)127<2204:FASOCR>2.0.CO;2.

Kharuk, V.I., Dvinskaya, M.L., Im, S.T., Golyukov, A.S. and Smith, K.T. (2022) 'Wildfires in the Siberian Arctic', *Fire*, 5(4), pp. 1–16. Available at: https://doi.org/10.3390/fire5040106.

Kharuk, V.I., Mariya, L.D., Ilya, A.P., Sergei, T.I. and Kenneth, J.R. (2016) 'Larch Forests of Middle Siberia: Long-Term Trends in Fire Return Intervals', *Regional Environmental Change*, 16(8), pp. 2389–2397. Available at: https://doi.org/doi:10.1007/s10113-016-0964-9.

Knorr, W., Kaminski, T., Arneth, A. and Weber, U. (2014) 'Impact of human population density on fire frequency at the global scale', *Biogeosciences*, 11(4), pp. 1085–1102. Available at: https://doi.org/10.5194/bg-11-1085-2014.

Latham, D. and Schlieter, J. (1989) 'Ignition probabilities of wildland fuels based on simulated lightning discharges', *United States Department of Agriculture, Forest Service*, (Research Paper INT-411), p. 16. Available at: http://www.firemodels.org/downloads/behaveplus/publications/Latham_and_Schlieter_INT-411_1989_ocr.pdf.

Latham, D. and Williams, E. (2001) 'Lightning and Forest Fires', *Monthly Weather Review*, 51(11), pp. 566–567. Available at: https://doi.org/10.1175/1520-0493(1923)51<566:laffic>2.0.co;2.

Li, F., Val Martin, M., Andreae, M.O., Arneth, A., Hantson, S., Kaiser, J.W., Lasslop, G., Yue, C., Bachelet, D., Forrest, M., Kluzek, E., Liu, X., Mangeon, S., Melton, J.R., Ward, D.S., Darmenov, A., Hickler, T., Ichoku, C.,

Magi, B.I., Sitch, S., Van Der Werf, G.R., Wiedinmyer, C. and Rabin, S.S. (2019) 'Historical (1700-2012) global multi-model estimates of the fire emissions from the Fire Modeling Intercomparison Project (FireMIP)', *Atmospheric Chemistry and Physics*, 19(19), pp. 12545–12567. Available at: https://doi.org/10.5194/acp-19-12545-2019.

Peterson, D.L. and Ryan, K.C. (1986) 'Modeling postfire conifer mortality for long-range planning', *Environmental Management*, 10(6), pp. 797–808. Available at: https://doi.org/10.1007/BF01867732.

Pyne, S.J., Andrews, P.L. and Laren, R.D. (1996) 'Introduction to Wildland Fire'. Canada: John Wiley & Sons, Inc.

Romps, D.M., Seeley, J.T., Vollaro, D. and Molinari, J. (2014) 'Projected increase in lightning strikes in the united states due to global warming', *Science*, 346(6211), pp. 851–854. Available at: https://doi.org/10.1126/science.1259100.

Rothermell, R.C. (1972) 'A Mathematical Model for Predicting Fire Spread', *United States Departament of Agriculture. Forest Service Research Paper*, p. 46.

Running, S.W., Nemani, R.R. and Hungerford, R.D. (1987) 'Extrapolation of synoptic meteorogical data in mountanious terrain and its use for simulating forest evapotranspiration and photosynthesis', *Canadian Journal of Forest Research* [Preprint]. Available at: https://doi.org/doi.org/10.1139/x87-081.

Sato, H., Itoh, A. and Kohyama, T. (2007) 'SEIB-DGVM: A new Dynamic Global Vegetation Model using a spatially explicit individual-based approach', *Ecological Modelling*, 200(3–4), pp. 279–307. Available at: https://doi.org/10.1016/j.ecolmodel.2006.09.006.

Schulzweida, U. (2019) 'CDO User Guide', (August). Available at: https://doi.org/10.5281/zenodo.3539275.

Sofronov, M.A., Volokitina, A.V. and Shvidenko, A.Z. (1998) 'Wildland fires in the north of Central Siberia', *The Commonwealth Forestry Review*, 77(2), pp. 124–127.

Thonicke, K., Spessa, A., Prentice, I.C., Harrison, S.P., Dong, L. and Carmona-Moreno, C. (2010) 'The influence of vegetation, fire spread and fire behaviour on biomass burning and trace gas emissions: Results from a process-based model', *Biogeosciences*, 7(6), pp. 1991–2011. Available at: https://doi.org/10.5194/bg-7-1991-2010.

Thonicke, K., Venevsky, S. and Sitch, S. (2001) 'The role of fire disturbance for global vegetation dynamics: coupling fire into a Dynamic Global Vegetation Model', *Global Ecology & Biogeography*, 10, pp. 661–677.

Venevsky, S., Thonicke, K., Sitch, S. and Cramer, W. (2002) 'Simulating fire regimes in human-dominated ecosystems: Iberian Peninsula case study', *Global Change Biology*, 8(10), pp. 984–998. Available at: https://doi.org/10.1046/j.1365-2486.2002.00528.x.

Viegas, D.X., Viegas, T.S.P. and Ferreira, D. (1992) 'Moisture content of fine forest fuels and fire occurrence in central portugal', *International Journal of Wildland Fire*, 2(2), pp. 69–86. Available at: https://doi.org/10.1071/WF9920069.

Williams, R.J., Gill, A.M. and Moore, P.H.R. (1998) 'Seasonal changes in fire behaviour in a tropical savanna in Northern Australia', *International Journal of Wildland Fire*, 8(4), pp. 227–239. Available at: https://doi.org/10.1071/WF9980227.

Wilson, R.A. (1982) 'A Reexamination of Fire Spread in Free-Burning Porous Fuel Beds', *United States Department of Agriculture, Forest Service* [Preprint].

Xu, W., Scholten, R.C., Hessilt, T.D., Liu, Y. and Veraverbeke, S. (2022) 'Overwintering fires rising in eastern Siberia', *Environmental Research Letters*, 17(4). Available at: https://doi.org/10.1088/1748-9326/ac59aa.